

Politecnico di Torino

Dipartimento di Ingegneria Strutturale, Edile e Geotecnica

Corso di Laurea Magistrale in Ingegneria Civile

The influence of the transverse distribution of loads in fatigue life of bridges



Relatore:

Giuseppe Carlo Marano

Candidato:

Gabriel Stecchi

Correlatori:

Rebecca Asso

Davide Masera

A.A. 2022/2023

Abstract

Most bridges that were built during the 1960s - 1980s were mainly designed in prestressed concrete. Nowadays, they represent about the 95% of the total number of bridges that are part of the Italian national transport network under the responsibility of private and public management companies. Existing bridges are naturally subjected to degradation mechanisms during their service life, due to environmental and operational events, leading to a decrease in performance, if also mechanical problems related to the transversal distribution of loads are added to this, serious problems can arise. It is important to underline that the development of stresses and the transfer of loads in a beam bridge is directly related to the relationship between transverse beams and longitudinal beams, in fact, the main structural function of cross-beams is to allow the correct transfer of loads in the transversal direction from the point of application of the load to the neighbouring beams. Improper mechanical interaction between the two elements leads to an insufficient transfer of loads, leading to a concentration of stresses generally applied to the edge beams. The goal of this Thesis, developed with the collaboration of the engineering company Masera Engineering Group, is to investigate the role of the transverse beams of an existing beam bridge in order to study the effective grade of loads transfer and to evaluate the fatigue behaviour of the structure.

Ringraziamenti

Sono finalmente giunto alla fine di questo percorso. È una frase che racchiude in sé gioia, soddisfazione e un pizzico di malinconia. In questi sei anni ho avuto la straordinaria fortuna di conoscere e apprezzare tante persone, le quali mi hanno permesso di diventare chi sono oggi. Per primi ringrazio i miei genitori, non basterebbero mille parole per descrivere le qualità che vi rendono dei genitori fantastici, tutto ciò che sono e tutto ciò che ho raggiunto lo devo a voi e all'amore che mi dimostrano ogni giorno. Ringrazio mia sorella per essere così diversa da me e per permettermi di vedere un mondo più colorato attraverso i suoi occhi.

Ci tengo poi a ringraziare Greta, Ilaria, Visco, Bomp e Martina, gli amici di sempre, quelli che nonostante i cambiamenti della vita non smettono mai di essere presenti, vi considero parte della mia famiglia.

Ringrazio Stefano per esserci sempre nonostante gli impegni e la distanza. Ringrazio Alice per essere l'amica che non mi aspettavo ma di cui non posso più fare a meno. Ringrazio Giulia V., Francesca, Giulia A., Riccio, Marina, Simone, Benni, Frank, Albi, Johnny, Enri, Laura, Alba, Raffaele.

Un grazie particolare va a Maurizio, non ce l'avrei mai fatta senza di te. Ne abbiamo passate tante, tantissime, ti considero un fratello e ti auguro il meglio.

Mentre scrivo queste righe non posso fare a meno di sentirmi molto fortunato, ci sarebbero tantissime persone da citare e tantissime cose da dire, ma la sintesi non è il mio forte e vedo la fine della pagina avvicinarsi.

Per ultimo, a costo di sembrare arrogante, voglio ringraziare me stesso, per non aver mai mollato ed essermi sempre rialzato nonostante le difficoltà e i fallimenti.

“Per quanto il vento ululi forte, una montagna non può inchinarsi a esso” - Mulan [2].

Contents

Abstract	I
Ringraziamenti	III
Contents	V
List of Figures	VIII
1 INTRODUCTION	1
1.1 Background	1
1.2 Scope of the Research	2
1.3 Thesis Overview	2
2 Overview of Beam Bridges	3
2.1 Structural Typologies	3
2.2 Construction Methods	6
2.3 Transverse distribution of loads	9
2.3.1 Courbon method	9
2.3.2 Guyon-Massonnet-Bares	12
2.3.3 Finite element method	13
3 Description of the Case Study	14
3.1 Location	14
3.2 Geometric Characteristics	14
3.2.1 Main Beams	15

3.2.2	Cross-Beams	17
3.2.3	Concrete Slab	18
3.2.4	Piers	18
3.2.5	Foundations	20
3.3	Used Materials Properties	20
4	Finite Element Structural Analysis	22
4.1	Model Description	22
4.1.1	Loads	22
4.1.1.1	Permanent Structural Loads (G1)	23
4.1.1.2	Permanent Non-Structural Loads (G2)	26
4.1.1.3	Wind Action	26
4.1.1.4	Thermal Action	33
4.1.1.5	Traffic Action	37
4.1.1.6	Load Combinations	40
4.1.2	Geometry	42
4.1.3	Boundary Conditions	42
4.2	Model Validation	43
4.3	Loads Transverse Distribution Analysis Results	46
5	Fatigue Analysis	53
5.1	Introduction to the Fatigue Phenomenon	53
5.1.1	Microscopic aspects of fatigue	55
5.1.2	Fatigue in reinforced concrete members	57
5.1.3	Fatigue analysis methods	58
5.2	Fatigue of concrete under compression	60
5.3	Influence of the transverse distribution of loads	62
5.3.1	Fatigue Load combination	62
5.3.2	Definition of Case 0 and Overloaded Case	64
5.3.3	Definition of concrete S-N curves	67

5.3.3.1	Kim & Kim proposal	67
5.3.3.2	Fib Model Code 2010	69
5.3.4	Discussion of the obtained results	71
5.3.4.1	Kim&Kim S-N curves results	71
5.3.4.2	fib Model Code 2010 S-N curves results	72
5.3.4.3	Models Comparison	73
	Conclusions	78
	Bibliography	A
	Acronyms	F

List of Figures

2.1	Simply supported girder	4
2.2	Gerber half-joint girder	4
2.3	Continuous Girder	5
2.4	Lifting construction method	6
2.5	Stationary formwork construction method	7
2.6	Incremental launching construction method	8
2.7	Balanced cantilever construction method	8
2.8	Courbon static scheme	10
3.1	Central span plan	15
3.2	Main Beam cross-section	15
3.3	Main Beam reinforcement	16
3.4	Main Beam prestress	16
3.5	Cross-beam cross-section	17
3.6	Cross-beam prestress	17
3.7	Pier cross-section	18
3.8	Pier capital	19
3.9	Pier elevation	20
3.10	Restraints configuration	20
4.1	Definition of l_0	23
4.2	Effective flange width parameters	24
4.3	Beam complex cross-section	24
4.4	Cross-beam complex cross-section	24

4.5	Effective Width overview	25
4.6	Parameters values: νb_0 , a_0 , k_s	27
4.7	Parameters for the exposure coefficient definition	29
4.8	Class of roughness of the terrain	29
4.9	Parameters for the exposure coefficient definition	30
4.10	Force Coefficient	31
4.11	$T_{e,min}$ and $T_{e,max}$ recommended values	34
4.12	Recommended values of linear temperature difference component	35
4.13	Recommended values of k_{sur} to account for different surfacing thickness	35
4.14	Load Model 1	37
4.15	Load Model 2	38
4.16	Number and width of notional lanes	38
4.17	Notional lanes representation	39
4.18	Partial Safety Factors for ULS Assessment	40
4.19	Combination coefficients for ULS Assessment	41
4.20	SAP2000 Model Plan	42
4.21	Restraints Configuration	42
4.22	Scheme 1 - C.M. LL.PP. n. 384, 1962	44
4.23	Scheme 5 - C.M. LL.PP. n. 384, 1962	44
4.24	Scheme 1 and Scheme 5 application	45
4.25	SAP2000 Model Plan	46
4.26	Bending Moment Diagram - Cross-Beam B	46
4.27	Bending Moment Diagram - Cross-Beam C	47
4.28	Bending Moment Diagram - Cross-Beam D	47
4.29	Bending Moment Diagram - Main Beam 1	48
4.30	Bending Moment Diagram - Main Beam 2	48
4.31	Bending Moment Diagram Comparison - Main Beam 1	49
4.32	Bending Moment Diagram Comparison - Main Beam 2	49
4.33	Main Beam simplified static scheme	50

4.34	Loading case	50
4.35	Influence of the cross-beams on ΔM	51
5.1	Fatigue stress cycle	54
5.2	Spectra of fatigue load categories [19]	55
5.3	Dislocation movement	55
5.4	Decreasing stiffness of concrete due to strain softening	57
5.5	Fatigue Load Model 1	62
5.6	Set of lorries for Fatigue Load Model 2	63
5.7	Bending moment difference between beam 1 and beam 2	64
5.8	Overload for Case Study	65
5.9	State of stress of the mid-span cross-section	66
5.10	S-N curve (Kim&Kim) [27]	68
5.11	S-N curve (fib Model Code 2010)	70
5.12	Kim&Kim results for study case	71
5.13	fib Model Code results for study case	72
5.14	Kim&Kim results comparison	74
5.15	fib Model Code results comparison	74

CHAPTER

1

INTRODUCTION

1.1 Background

The majority of the bridge and viaducts in Italy were designed and realized between the 1960s and the 1980s, following regulations and code rules valid at that time, considering lower volumes of traffic than those present today and with limited knowledge about the behaviour of complex structures such as bridges and viaducts. The typology of bridges that was most present, was realized using concrete beams as the support structure of the deck (Beam Bridges), because of their speed and simplicity of construction and the possibility of easy prefabrication of the structural elements.

Nowadays those bridges are getting to the end of their service life showing cases of high degradation due to environmental actions and different loading conditions compared to those present at construction time. The level of technology available at that time, regarding the connection between the cross-beams and the main beams, affects the transverse distribution of the loads, causing concentration of bending and shear stresses at the edge beams [14]. This condition, in addition to the increase of traffic action in the last years, leads to several problems that concern the durability and fatigue life of the structure, which is directly influenced by the dynamic action of the traffic.

1.2 Scope of the Research

The aim of the thesis is to study the influence of the cross-beams in the transverse load's distribution of an existing bridge and to create a representative model of the structure, allowing to study the current behaviour of the bridge under the action of today's traffic loads, focusing on the fatigue behaviour of the structure. The proposed model will be realized using the finite element program SAP2000 and using the original design documentation of the bridge. The thesis allows comprehending the behaviour of a beam bridge designed more than 40 years ago under the effects of today's loads allowing to individuate problems related to the key function of the cross-beams.

1.3 Thesis Overview

The first two chapters of this thesis are devoted to a general overview of beam bridges in terms of structural typologies, construction methods and methods of calculations, while in the third chapter, the case of study is presented focusing on geometric characteristics and used materials. In the fourth chapter the finite element model of the case study is fully described referring to the geometry, the applied loads and the boundary conditions, afterwards it is explained how the model was validated and finally, the influence of the cross-beams in the transverse load's distribution is studied. The fifth chapter presents the fatigue phenomenon and the fatigue analysis performed on the case study.

2

Overview of Beam Bridges

2.1 Structural Typologies

A beam bridge is a typology of bridge structure widely used because of its construction speed and simplicity and the possibility of easy prefabrication of the structural elements. The main elements composing such a structure are:

- **Main beams (or longitudinal beams):** these elements are the ones carrying the highest loads coming from the superstructure and transferring them to the piers. They generally have an I or V cross-section shape, they may be cast-in-place or precast and may be realized with or without prestress;
- **Cross-beams (or transverse beams):** are usually cast-in-place and connected to the longitudinal beams by means of reinforcing or prestressing steel, they can be connected or not with the slab. The main structural function of these elements is to allow the correct transverse distribution of the loads between the main beams.
- **Concrete slab:** it is supported by the grid composed of the main beams and the cross-beams, it has the main structural function to transfer the live loads and the traffic loads to the cross-beams and to sustain the local effects of loading.

The advantages and disadvantages of a beam bridge are strictly related to the structural system typology, in particular, it is possible to define three main typologies:

- Simply Supported Beams

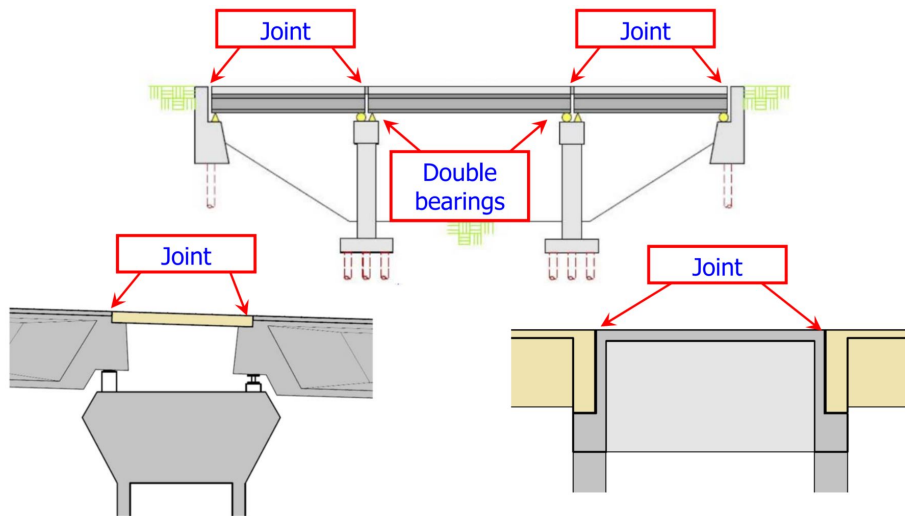


Figure 2.1: Simply supported girder

A simply supported beam is a very common system which employs double bearings per pier in addition to a wide use of connection joints between the different spans. The main advantages are related to the simplicity of the pre-cast of the structural elements and the simplicity and speed of the construction process, moreover simply supported beams are isostatic structures and therefore insensitive to differential settlements at the support and to the temperature variation. On the other hand, this typology of structure allows only the construction of spans of limited length, in addition of that there is a large use of short service life components such as bearings and joints which lead to problems of durability.

- Bridges with Gerber beam Half-Joints

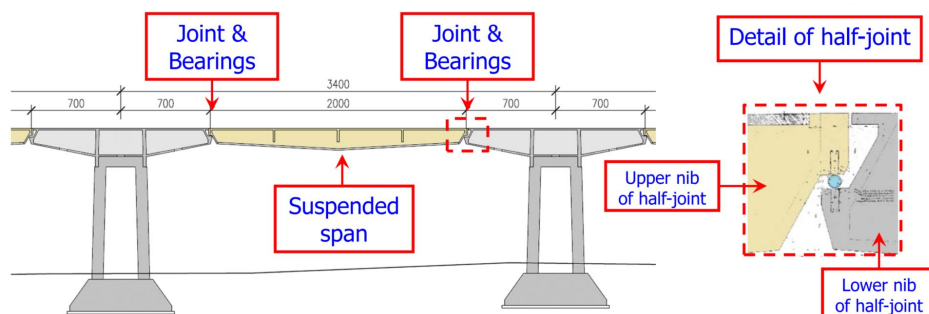


Figure 2.2: Gerber half-joint girder

The Gerber beam half-joint is characterised by the presence of a suspended span interposed between two pier segments. The main advantages and drawbacks are almost the same as the simply supported beam but it is important to mention that in this type of system, there is a better use of employed materials though there is an evident larger use of short service life elements and therefore more problems in terms of the durability of the structural components.

- Continuous Beams

► **Continuous girder**

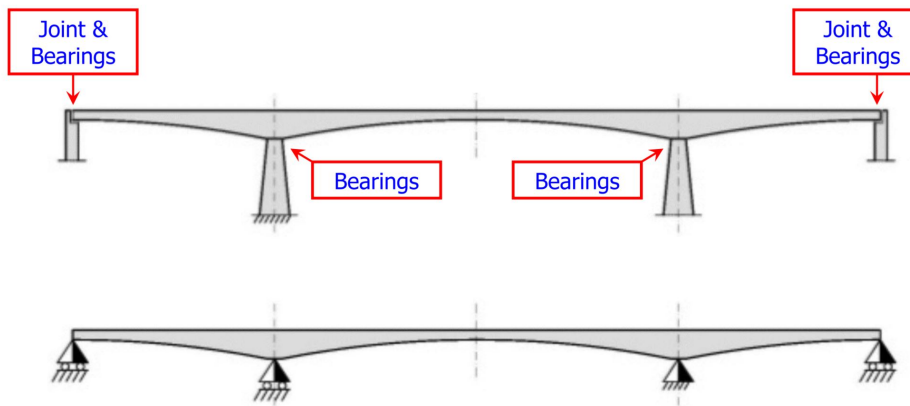


Figure 2.3: Continuous Girder

The continuous beam system allows the realisation of bridges with longer spans, moreover, in this system, the components having a short service life are present in a very low number, therefore the problems related to durability are less than in the previous systems. Nevertheless, it is more complicated to pre-cast a continuous beam, moreover, design and construction processes are more challenging, lastly, unlike previous systems continuous beams are particularly sensitive to settlements at the supports and to temperature variations due to the fact that continuous beams are hyperstatic structures.

2.2 Construction Methods

Since the 1960s, the construction methods for bridges have developed more and more, and nowadays technical and technological achievement allows to considerably reduce costs, time and resources wasted, in addition of that the experience related to the design of key infrastructures such as bridges has led to an increase of efficiency of the design of this type of structures. When dealing with a bridge structure it is important to consider the peculiarities of this type of structure. A bridge has generally a plane shape which spreads in length, therefore the characteristics of the foundation ground may vary consistently and consequently also the height of the supports (piers) may range from a few meters to dozen of meters. Lastly, the amount and the magnitude of live loads are extremely higher than other buildings for civil use. From a construction point of view, a bridge can be erected using several methodologies:

- **Lifting:** This technique involves the use of cranes to place the elements composing the superstructure of the bridge after the realization of the vertical elements, sometimes the morphology of the terrain hampers the use of this method.



Figure 2.4: Lifting construction method

- **Stationary formwork:** In this method, the concrete elements are realized in situ using temporary stationary falsework directly supported on the ground, it provides a stable work platform upon which the concrete forms are set, moreover it gives additional support to the concrete superstructure until it has achieved the sufficient strength to support itself [48].



Figure 2.5: Stationary formwork construction method

- **Traveling formwork:** In this case, the falsework is supported by temporary piers resting on the ground over rollers or on main steel beams supported on brackets attached to the final piers (advancing shoring system) [51].
- **Horizontal incremental launching:** This method is used for the construction of segmental bridges, the segments composing the superstructure are manufactured in a casting yard located behind one or both bridge abutments. Each segment is prestressed and launched using jacks over the piers heads which have to be provided with temporary sliding bearings [30]. It is preferable to have a bridge with a straight profile, although limited curvature can be managed.



Figure 2.6: Incremental launching construction method

- Cast-in-situ balanced cantilever construction: The first segment above the closest pier to the centreline is realized, and then two form travellers are erected on the two sides of it to work as supports for the realization of the next segments. The segments are realized symmetrically to the pier in order to ensure balance. After the casting of the two new segments prestress is applied and the travellers are moved to the next position, the same process is repeated until both cantilever ends are completed [51].



Figure 2.7: Balanced cantilever construction method

The identification of the most suitable is directly related to the used materials, construction typology and site morphology.

2.3 Transverse distribution of loads

Considering the typologies of beam bridges already seen it is possible to notice that one of the crucial aspects is related to durability and it is also affected by the high number of short service life elements such as bearings and joints. In addition to that also water infiltration is a huge problem which strongly affects the durability of bridges. Sometimes damages and degradation of the structural elements are due to atmospheric precipitations, but in some cases, it can be noticed that the state of degradation, which can manifest itself in the form of advanced cracking states in structural elements such as beams and concrete slabs, can be traced back to an increase of the flexural, shear and/or torsional stresses due to defects which are difficult to spot during the design process. [14]. The development of stresses and the transfer of loads in a beam bridge is directly related to the relationship between transverse beams and longitudinal beams, in fact, the main structural function of cross-beams is to allow the correct transfer of loads in the transversal direction from the point of application of the load to the neighbouring beams. Improper mechanical interaction between the two elements leads to an insufficient transfer of loads and causes a concentration of stresses generally applied to the edge beams. [14]. Depending on the position of the live load on the deck slab, the transverse distribution of loads varies in each beam, this distribution can be estimated using several methods.

2.3.1 Courbon method

The transverse distribution of the loads in a beam bridge is affected by the flexural rigidity and the torsional rigidity of the beams, the latter generally depends upon the effectiveness of the cross-beams[17]. The hypothesis of the Courbon method include[8]:

- The torsional rigidity of the main beams is considered equal zero $\gamma_p = 0$;
- The flexural rigidity of the cross-beams connecting the main beams is considered infinite $\rho_e = \infty$.

These hypotheses allow to consider the cross-beam as a continuous beam supported by elastic springs representing the main beams[39]:

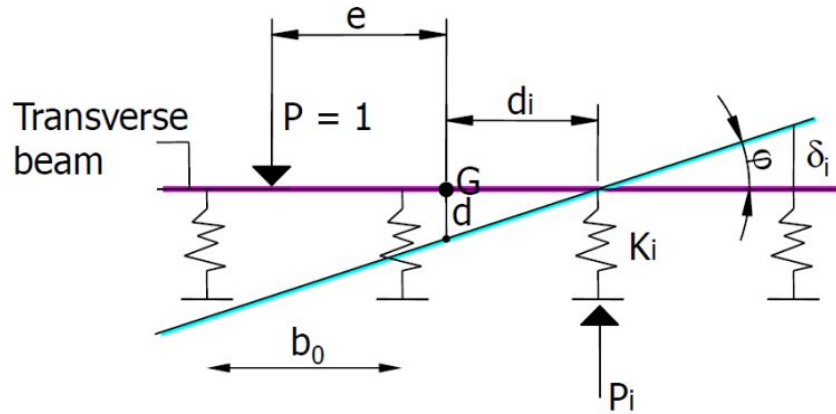


Figure 2.8: Courbon static scheme

In the static scheme above G represent the rigidity gravity centre of the springs system, δ is the displacement of the cross-beam and ϕ is the corresponding rotation angle. The total displacement of the beam is:

$$\delta_i = \delta + \phi \cdot d_i \quad (2.1)$$

where:

- δ is the vertical displacement;
- ϕ is the rotation angle;
- d_i is the distance from the rigidity gravity centre G of the i -th spring.

The generic applied force is:

$$P_i = K_i \cdot \delta_i = K_i \cdot (\delta + \phi \cdot d_i) \quad (2.2)$$

where K_i is the elastic constant of the i -th spring. Imposing the equilibrium in the vertical direction:

$$\sum_{i=1}^n P_i = 1 \quad (2.3)$$

substituting (2.2) into (2.3):

$$\sum_{i=1}^n (K_i \cdot \delta + K_i \cdot \phi d_i) = \delta \cdot \sum_{i=1}^n K_i + \phi \cdot \sum_{i=1}^n K_i \cdot d_i = 1$$

and having that $\sum_{i=1}^n K_i \cdot d_i = 0$ because G is the centroid of the rigidities, it is possible to obtain that:

$$\delta = \frac{1}{\sum_{i=1}^n K_i} \quad (2.4)$$

Similarly applying the rotation equilibrium:

$$\sum_{i=1}^n P_i \cdot d_i = 1 \cdot e \quad (2.5)$$

where e is the eccentricity of the applied load P with respect to G. Then substituting (2.2) into (2.5):

$$\sum_{i=1}^n (K_i \cdot \delta + K_i \cdot \phi d_i) \cdot d_i = \delta \cdot \sum_{i=1}^n K_i \cdot d_i + \phi \cdot \sum_{i=1}^n K_i \cdot d_i^2 = 1 \cdot e$$

and having also in this case that $\delta \cdot \sum_{i=1}^n K_i \cdot d_i = 0$, it is possible to obtain:

$$\phi = \frac{e}{\sum_{i=1}^n K_i \cdot d_i^2} \quad (2.6)$$

If the main beams are identical and have the same restrains it's possible to assume that:

$$K_i = K = \text{const} \quad (2.7)$$

At this point, considering an applied load $P = 1$ and replacing (2.4), (2.6) and (2.7) into (2.2):

$$\rho_{i,e} = \frac{K_i}{\sum_{i=1}^n K_i} + \frac{K_i \cdot d_i \cdot e}{\sum_{i=1}^n K_i \cdot d_i^2} = \frac{K}{n \cdot K} + \frac{K \cdot d_i \cdot e}{K \cdot \sum_{i=1}^n d_i^2} = \frac{1}{n} + \frac{d_i \cdot e}{\sum_{i=1}^n d_i^2}$$

at the end it gives:

$$\rho_{i,e} = \frac{1}{n} + \frac{d_i \cdot e}{\sum_{i=1}^n d_i^2} \quad (2.8)$$

The eq.(2.8) is the Courbon distribution coefficient which represents the percentage of the load P , applied with an eccentricity of e from the centroid G of the rigidities, acting on the i -th main beam[39]. It is possible to demonstrate that the Courbon Method gives a good approximation of the transverse distribution of the loads between the main beams when[8]:

$$\frac{L}{b_0} > 10 \quad (2.9)$$

In which:

- L is the total length of the main beam;
- b_0 is the interaxle spacing between the beams.

2.3.2 Guyon-Massonnet-Bares

The method of Guyon-Massonnet-Bares is based on the use of a set of distribution coefficients, which allows considering the two extreme cases: the torsional rigidity is not considered or is fully considered, therefore enabling the determination of the actual load distribution of any type of bridge[36]. The distribution coefficient K depends upon the value of the flexural parameter of Guyon (θ) and the torsional parameter (α)[41]:

$$\theta = \frac{b}{l} \cdot \sqrt[4]{\frac{\rho_p}{\rho_e}} \quad (2.10)$$

$$\alpha = \frac{\rho_{txy} + \rho_{tyx}}{2 \cdot \sqrt{\rho_p \cdot \rho_e}} \quad (2.11)$$

in which:

- ρ_p is the flexural rigidity of the main beam;
- ρ_e is the flexural rigidity of the cross-beam;
- ρ_{txy} is the torsional rigidity per unit width of the deck;
- ρ_{tyx} is the torsional rigidity per unit length of the deck;
- b is the active semi-rigidity of the deck, defined by Bares-Massonnet as[17]:

$$2 \cdot b = n_p \cdot b_0 \quad (2.12)$$

in which n_p is the number of cross-beams;

- l is the total length.

The distribution coefficient K is then obtained by interpolation:

$$K = K_0 + K_1 - K_0 \cdot \sqrt{\alpha} \quad (2.13)$$

In which K_0 is obtainable from the Bares-Massonnet tables, while K_1 are defined in the Massonnet tables[17].

2.3.3 Finite element method

The Finite Element Method (FEM) is a well-known numerical method widely used for the solution of complicated structural engineering problems and it is also very useful to predict the bridge behaviour under traffic loads[43]. The FEM is based on the application of a discretization process of a continuous system[10], the steps which have to be followed are[12]:

- 1 - Idealization: the structure is defined in terms of geometry, applied loads, boundary conditions and material properties,
- 2 - Discretization: the FEM model is created, the structure is divided into a finite number of Finite Element (FE), which can be line elements, 2D elements or 3D elements, and the boundary conditions are applied on the model and the loading conditions and material properties are modelled as well;
- 3 - Finite Element Analysis (FEA): for each EF a stiffness matrix and a vector representing the equivalent nodal applied loads are defined. The stiffness matrices of the EF and the nodal load vectors are assembled and a system of equations having a number of unknowns equal to the total number of DOF of the structure is created. The external restraints are applied as a boundary condition of the system and the unknown nodal displacements are calculated.
- 4 - Post-processing: The obtained values of the nodal displacement are backwards substituted to obtain secondary unknowns: stresses and strains.

CHAPTER

3

Description of the Case Study

The aim of the following chapter is to give a general overview of the characteristics of the case of study that will be analysed in this thesis, in particular, the following pages are focused on the explanation of the geometrical characteristics of the bridge, the properties of the used materials and the main characteristics of the structural elements.

3.1 Location

The bridge is part of the Autostrada dei Fiori (A10) in the road section that links the city of Genova with Savona and it was realized in 1974.

3.2 Geometric Characteristics

The bridge is composed of a carriageway with three lanes (two of them for normal traffic and one for emergency) and it has a total width of 11.25 m with a constant transversal slope of 2%. The total length of the bridge is 126.50 m divided in the following way: a span of 41.25 m between the abutments and the axis of the immediately following pier and a central span of 44 m between the axis of the two piers, for the purpose of this study only the central span will be analysed:

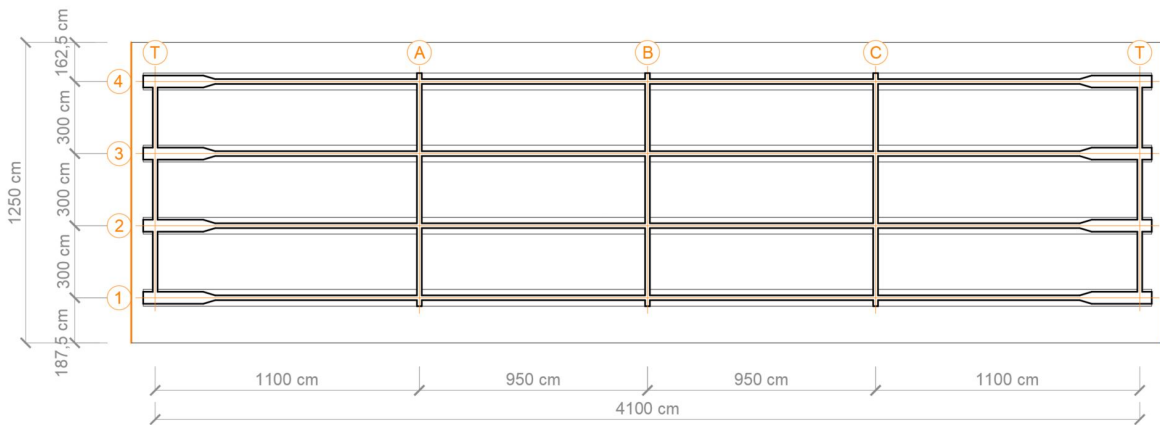


Figure 3.1: Central span plan

The structure is composed of four main beams connected with each other by three cross-beams along the span length and two cross-beams at the piers connection.

3.2.1 Main Beams

The longitudinal beams (main beams) are precast and realized in prestressed reinforced concrete class C35/45 with a length of 41 meters in the base span. The shape of the cross-section is a double T having the following dimensions:

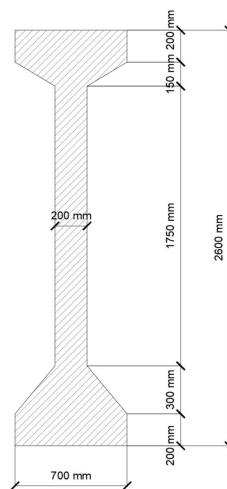


Figure 3.2: Main Beam cross-section

The reinforcement of the main beam is provided by steel reinforcement bars type ALE having $\phi = 10\text{mm}$ and the following configuration:

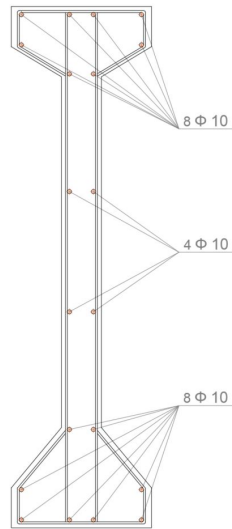


Figure 3.3: Main Beam reinforcement

The prestress is applied on the cross-section using tendos type Freyssinei 12T13:

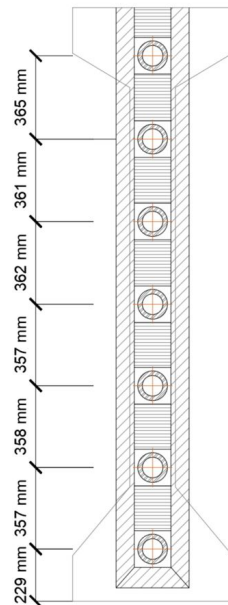


Figure 3.4: Main Beam prestress

3.2.2 Cross-Beams

The cross-beams are cast-in-place and realized in reinforced concrete class C35/45. The shape of the cross-section is a rectangle having the following dimensions:

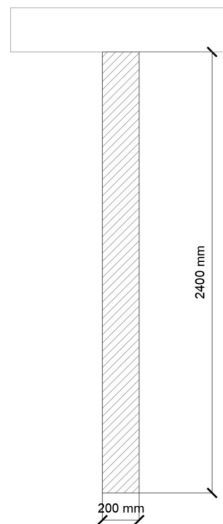


Figure 3.5: Cross-beam cross-section

The prestress is applied on the cross-section using 3 strands $12\phi 7$ placed at 0.81, 1.21 and 1.61 meters from the top of the deck slab:

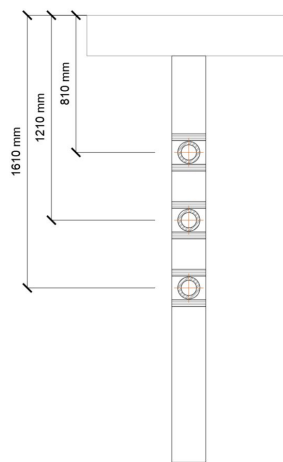


Figure 3.6: Cross-beam prestress

3.2.3 Concrete Slab

The concrete slab is cast-in-place using a concrete C35/45 and has a thickness of 24 cm. It is connected both with the main and cross-beams and is adequately reinforced using steel bars type ALE having a diameter $\phi = 12\text{mm}$

3.2.4 Piers

The two piers of the bridge have a box-section reinforced concrete C20/25 shaft having two trapezoidal compartments, each pier supports a monolithic capital realized in reinforced concrete C20/25 as well:

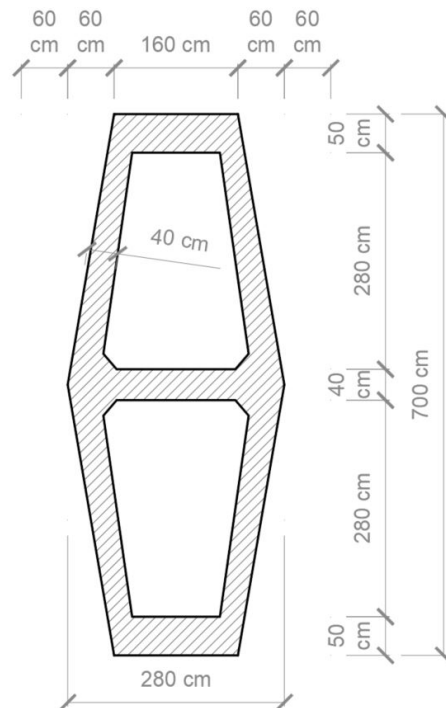


Figure 3.7: Pier cross-section

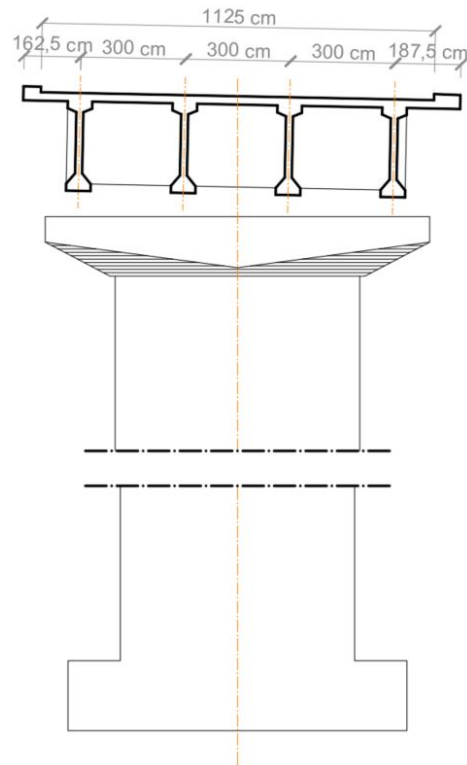


Figure 3.8: Pier capital

The steel bearings used as supports for the longitudinal beams are of two typologies:

- Fixed hinge.
- Unidirectional roller.

Four fixed hinges are located at the abutments, while on the shorter pier, there are four fixed supports and four mobile supports, on the higher pier all the supports are fixed. A representation of the bearings configuration is reported in the figures below:

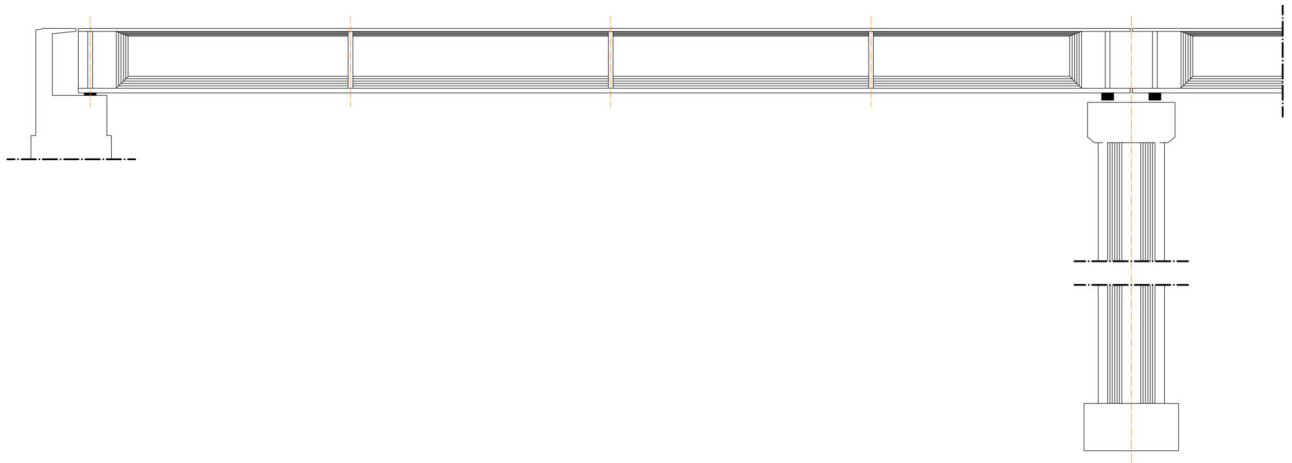


Figure 3.9: Pier elevation

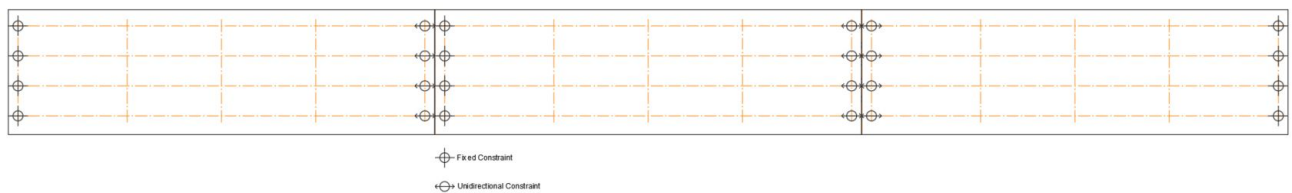


Figure 3.10: Restrains configuration

3.2.5 Foundations

The pier foundation is realized on a bedrock with an high cohesion and bearing capacity. The foundation itself is a monolithic reinforced concrete block having dimension $10 \times 4 \text{ m}^2$ and 4 meters height.

3.3 Used Materials Properties

The main beams and the cross-beams are made of reinforced concrete class C35/45 prestressed using harmonic steel for the tendons and strands: 8 tendons 12T13 Freyssinet type and 3 strands $12\phi 7$ respectively. The piers are made of concrete class C20/25. The steel used for the reinforcement is a type ALE. The main features of the implemented construction materials are reported in the tables below:

Concrete [C35/45]	
R_{ck} [MPa]	45
f_{ck} [MPa]	37.35
f_{cm} [MPa]	35.67
f_{ctm} [MPa]	2.74
$f_{ctk_{0.05}}$ [MPa]	1.92
E_{cm} [MPa]	32218
ν_s [MPa]	0.2
α_{cc}	1.00
γ_c	1.00
FC	1.35
f_{cd} [MPa]	27.67
f_{ctd} [MPa]	1.92
f_{bd} [MPa]	3.03

Table 3.1: Concrete C35/45 properties

Reinforcing Steel (ALE)	
f_{yk} [MPa]	440
f_{tk} [MPa]	506
E_s [MPa]	210000
γ_s	1.00
FC	1.35
f_{yd} [MPa]	325.9

Table 3.2: Steel Ale properties

12 T 13 Freyssinet (Tendons)	
d [mm]	-
A [mm^2]	1130
$f_{p(1)k}$ [MPa]	1670
f_{ptk} [MPa]	1750
E_p [MPa]	210000
σ_{spi} [MPa]	1146.6
σ_{spf} [MPa]	890
N° of cables	8
A_p [mm]	9040
Relaxation coeff.	8%
μ	0.19
γ_s	1.15
FC	1.35
f_{pyd} [MPa]	1237

Table 3.3: Harmonic steel (Freyssinet) properties

Harmonic Steel (Strands)	
d [mm]	7
A [mm^2]	77
$f_{p(0.1)k}$ [MPa]	1420
f_{ptk} [MPa]	1650
E_p [MPa]	210000
σ_{spi} [MPa]	-
σ_{spf} [MPa]	-
N° of cables	12
A_p [mm]	923.60
Relaxation coeff.	8%
μ	0.19
γ_s	1.15
FC	1.35
f_{pyd} [MPa]	1051.9

Table 3.4: Harmonic steel properties

4

Finite Element Structural Analysis

4.1 Model Description

In the following chapter it is explained and defined the finite element model used during the structural analysis process. The model itself was created using the software SAP2000.

4.1.1 Loads

The structural analysis performed on the model is considering the applied loads as follows [20]:

- Permanent structural loads (G1), are considered as the loads due to the self-weight of the elements composing the structure (e.g.: beams, slabs);
- Permanent non-structural loads (G2), are considered as the loads due to the self-weight of non-structural elements having other specific functions (e.g.: kerbs, traffic barriers, pavement);
- Environmental loads, such as wind action and temperature action.
- Live loads, more specifically the loads due to the traffic action.

4.1.1.1 Permanent Structural Loads (G1)

The permanent loads (G1) considered are the self-weight of the structural elements, in particular longitudinal beams, cross-beams and the concrete slab. To create a simplified model and in order to consider the stiffness provided by the concrete slab, it was set to include the collaborating slab portion in the beam section, to do that it was necessary to calculate the effective width (b_{eff}) of each of the four longitudinal beams to define a complex section. The effective width of the flange of a T beam cross-section defines the area in which the uniform condition of stress can be assumed [31], it generally depends upon web and flange dimension, type of loading, span length, support conditions, and transverse reinforcement. Following the EC2 sec. - 5.3.2 [46] the b_{eff} was calculated for the generic beam as follows:

$$b_{eff} = \sum b_{eff,i} + b_w \leq b \quad (4.1)$$

where:

- b_w is the width of the cross-section flange;
- $b_{eff,i}$ is the effective width component, calculated as:

$$b_{eff,i} = 0.2 \cdot b_i + 0.1 \cdot l_0 \leq 0.2 \cdot l_0 \quad (4.2)$$

The meaning of the various terms is represented in the figures below:

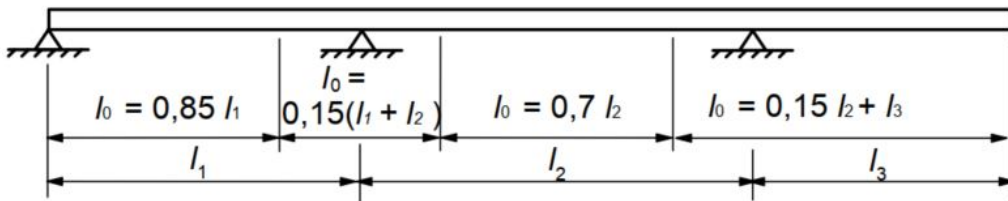


Figure 4.1: Definition of l_0

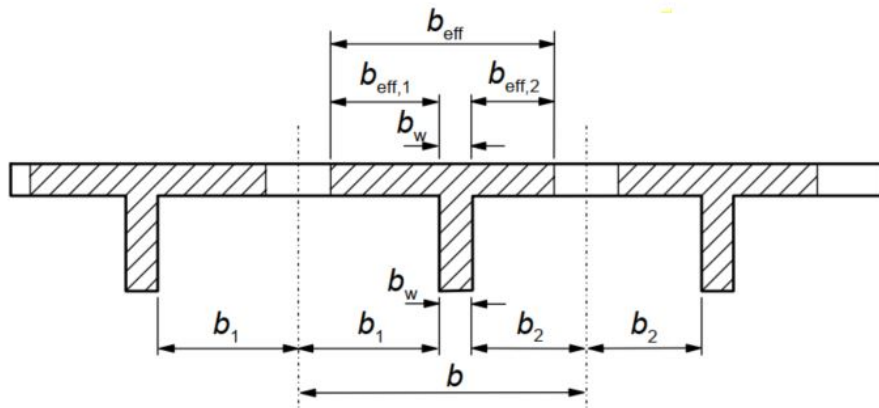


Figure 4.2: Effective flange width parameters

Considering the cross-section of a generic longitudinal beam, it was possible to calculate for each beam the effective width in order to obtain the following results:

Effective Width Calculation Results								
Element	l_0 [m]	b [m]	b_w [m]	b_1 [m]	b_2 [m]	$b_{eff,1}$ [m]	$b_{eff,2}$ [m]	b_{eff} [m]
Beam 1	41	-	0.20	1.78	1.40	1.78	1.40	3.38
Beam 4	41	3.13	0.20	1.53	1.40	1.53	1.40	3.13
Beam 2-3	41	3.00	0.20	1.40	1.40	1.40	1.40	3.00
Cross-beam H	2.10	6.48	0.20	0.88	5.40	0.39	0.42	1.01
Cross-beam A-C	2.10	10.25	0.20	5.40	4.65	0.42	0.42	1.04
Cross-beam B	2.10	9.50	0.20	4.65	4.65	0.42	0.42	1.04

Table 4.1: Effective Width Calculation

Finally, the procedure leads to the definition of a complex cross-section composed of the real cross-section of each beam and the slab, whose width is set as the effective width of the concrete slab collaborating with the related beam.

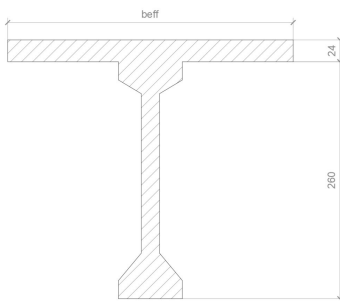


Figure 4.3: Beam complex cross-section

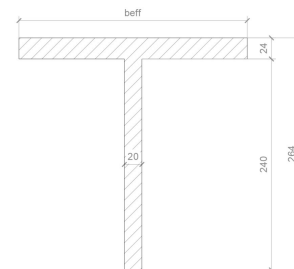


Figure 4.4: Cross-beam complex cross-section

A graphical representation of the effective width of each beam element and, in other words, the amount of concrete slab collaborating with it is presented below:

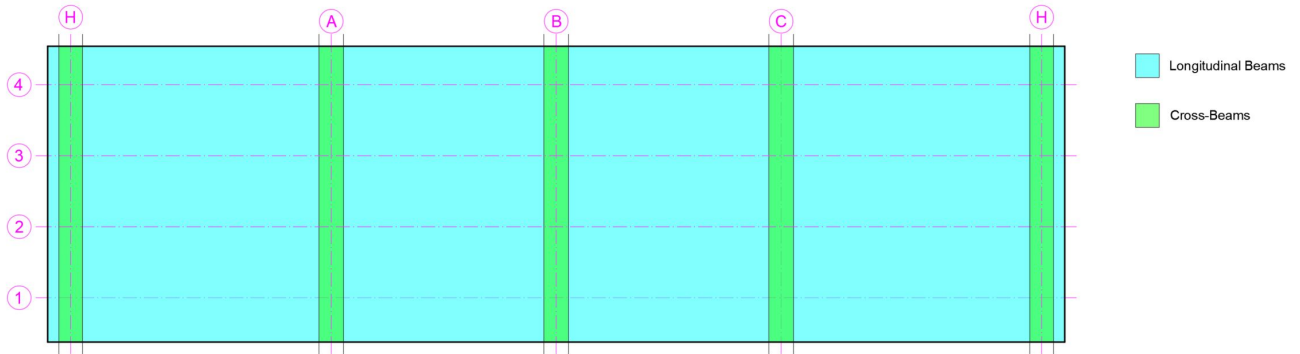


Figure 4.5: Effective Width overview

As it is possible to notice there is an overlapping area in correspondence of the cross-beams, therefore, it was resolved to multiply the mass of each cross-beam for a coefficient equal to the ratio between the weight of the original cross-section and the weight of the new cross-section, which included also the collaborating portion of the concrete slab, in order to avoid taking into consideration the weight of the concrete slab twice. By considering the overall area and the qualities of the material being utilised, it is now possible to determine the actual self of each beam:

Applied Structural permanent loads (G1)			
Element	Area [m^2]	γ [KN/m^3]	G1 [KN/m]
Beam 1	1.64	25	41.09
Beam 4	1.55	25	39.59
Beam 2-3	1.58	25	38.81
Cross-beam H	0.48	25	12
Cross-beam A-C	0.48	25	12
Cross-beam B	0.48	25	12

Table 4.2: Applied Structural Permanent Loads

4.1.1.2 Permanent Non-Structural Loads (G2)

For what concerns the permanent non-structural loads the elements that were considered are:

- Road pavement;
- Concrete kerb;
- Traffic barrier.

The road pavement applied on the bridge is a bitumen pavement with 25 cm of thickness, the distribution of the consequent load is applied on the longitudinal beams, and the two edge beams are also affected by the presence of the concrete kerb and the traffic barrier. For the concrete kerb, the related applied load is calculated considering the area of the kerb, which is $0.128 m^2$ and $0.085 m^2$ for beam 1 and beam 4 respectively. For what concerns the traffic barrier it was considered an integrated barrier with a load of 2 KN/m. All the permanent non-structural loads were summed up and applied as a unique distributed load on each beam:

Applied Non-Structural permanent loads (G2)				
Element	Pavement [KN/m]	Concrete curb [KN/m]	Traffic barrier [KN/m]	G2 [KN/m]
Beam 1	8.63	1.79	2	12.42
Beam 2-3	9.00	-	-	9.00
Beam 4	7.13	2.85	2	11.98

Table 4.3: Applied Non-Structural Permanent Loads

4.1.1.3 Wind Action

To determine the wind action on the bridge is taken as reference the D.M. 17/01/2018 §3.3 [49] and what is reported in the explanatory circular. The wind action induces loads that are variable in time and generate dynamic effects but it is generally considered as a distributed horizontal load. Following the previously mentioned code rules the calculation of the wind action is performed with the following steps:

- a) Reference Base Velocity

The reference base velocity v_b is the mean value considering a time of 10 minutes and

a height of 10 meters from the ground considering a homogeneous plain terrain and a design return period $T_R = 50 \text{ years}$. This velocity is defined as:

$$v_b = v_{b0} \cdot c_a \quad (4.3)$$

Where v_{b0} is the reference base velocity at the sea level, which is a function of the location of the site in which the structure is realized. The second parameter, c_a , is the altitude coefficient defined as:

– if $a_s \leq a_0$

$$c_a = 1 \quad (4.4)$$

– if $a_0 < a_s \leq 1500m$

$$c_a = 1 + k_s \cdot (a_s/a_0 - 1) \quad (4.5)$$

where a_0 and k_s are two parameters that are a functions of the site location and a_s is the altitude of the site where the construction takes place. The code rules give a table containing all the above parameters divided by geographic area:

Tab. 3.3.I - Valori dei parametri $v_{b,0}$, a_0 , k_s

Zona	Descrizione	$v_{b,0}$ [m/s]	a_0 [m]	k_s
1	Valle d'Aosta, Piemonte, Lombardia, Trentino Alto Adige, Veneto, Friuli Venezia Giulia (con l'eccezione della provincia di Trieste)	25	1000	0,40
2	Emilia Romagna	25	750	0,45
3	Toscana, Marche, Umbria, Lazio, Abruzzo, Molise, Puglia, Campania, Basilicata, Calabria (esclusa la provincia di Reggio Calabria)	27	500	0,37
4	Sicilia e provincia di Reggio Calabria	28	500	0,36
5	Sardegna (zona a oriente della retta congiungente Capo Teulada con l'Isola di Maddalena)	28	750	0,40
6	Sardegna (zona a occidente della retta congiungente Capo Teulada con l'Isola di Maddalena)	28	500	0,36
7	Liguria	28	1000	0,54
8	Provincia di Trieste	30	1500	0,50
9	Isole (con l'eccezione di Sicilia e Sardegna) e mare aperto	31	500	0,32

Figure 4.6: Parameters values: v_{b0} , a_0 , k_s

b) Reference Velocity

The reference base velocity v_r is the mean value considering a time of 10 minutes and a height of 10 meters from the ground having a homogeneous plain terrain and a design return period $T_r = 50$ years. This velocity is defined as:

$$v_r = v_b \cdot c_r \quad (4.6)$$

In which v_b is the reference base velocity and c_r is the return coefficient function of the return period T_R , in absence of further information the return period is taken equal to 50 years and therefore the return coefficient is taken equal to 1.

c) Reference Kinematic Pressure

The reference kinematic pressure is given by the following expression:

$$q_r = \frac{1}{2} \cdot \rho \cdot v_r^2 \quad (4.7)$$

In which v_r is the reference wind velocity and ρ is the air density conventionally assumed constant and equal to 1.25 kg/m^3 .

d) Exposure Coefficient

The exposure coefficient c_e depends upon z , defined as the height from the ground of the considered point, the morphology of the ground itself and the exposure category of the considered site where the structure takes place. Considering that there are no specific analyses and the height from the ground $< z = 200 \text{ m}$, it is possible to calculate c_e with the following formulas:

– if $z \geq z_{min}$:

$$c_e(z) = k_r^2 \cdot c_t \cdot \ln(z/z_0) \cdot [7 + c_t \cdot \ln(z/z_0)] \quad (4.8)$$

– if $z < z_{min}$:

$$c_e(z) = c_e(z_{min}) \quad (4.9)$$

in which c_t is the topographic coefficient, while k_r , z_0 and z_{min} are assigned parameters function of the exposure category of the site in which the structure takes place, in the table given by the code rules:

Tab. 3.3.II - Parametri per la definizione del coefficiente di esposizione

Categoria di esposizione del sito	K_r	z_0 [m]	z_{min} [m]
I	0,17	0,01	2
II	0,19	0,05	4
III	0,20	0,10	5
IV	0,22	0,30	8
V	0,23	0,70	12

Figure 4.7: Parameters for the exposure coefficient definition

The category of exposure is assigned considering the geographic position of the site and the class of roughness of the ground, both of them are defined by the code rules:

Tab. 3.3.III - Classi di rugosità del terreno

Classe di rugosità del terreno	Descrizione
A	Aree urbane in cui almeno il 15% della superficie sia coperto da edifici la cui altezza media superi i 15 m
B	Aree urbane (non di classe A), suburbane, industriali e boschive
C	Aree con ostacoli diffusi (alberi, case, muri, recinzioni,...); aree con rugosità non riconducibile alle classi A, B, D
D	a) Mare e relativa fascia costiera (entro 2 km dalla costa); b) Lago (con larghezza massima pari ad almeno 1 km) e relativa fascia costiera (entro 1 km dalla costa) c) Aree prive di ostacoli o con al più rari ostacoli isolati (aperta campagna, aeroporti, aree agricole, pascoli, zone paludose o sabbiose, superfici innevate o ghiacciate, ...)

L'assegnazione della classe di rugosità non dipende dalla conformazione orografica e topografica del terreno. Si può assumere che il sito appartenga alla Classe A o B, purché la costruzione si trovi nell'area relativa per non meno di 1 km e comunque per non meno di 20 volte l'altezza della costruzione, per tutti i settori di provenienza del vento ampi almeno 30°. Si deve assumere che il sito appartenga alla Classe D, qualora la costruzione sorga nelle aree indicate con le lettere a) o b), oppure entro un raggio di 1 km da essa vi sia un settore ampio 30°, dove il 90% del terreno sia del tipo indicato con la lettera c). Laddove sussistano dubbi sulla scelta della classe di rugosità, si deve assegnare la classe più sfavorevole (l'azione del vento è in genere minima in Classe A e massima in Classe D).

Figure 4.8: Class of roughness of the terrain

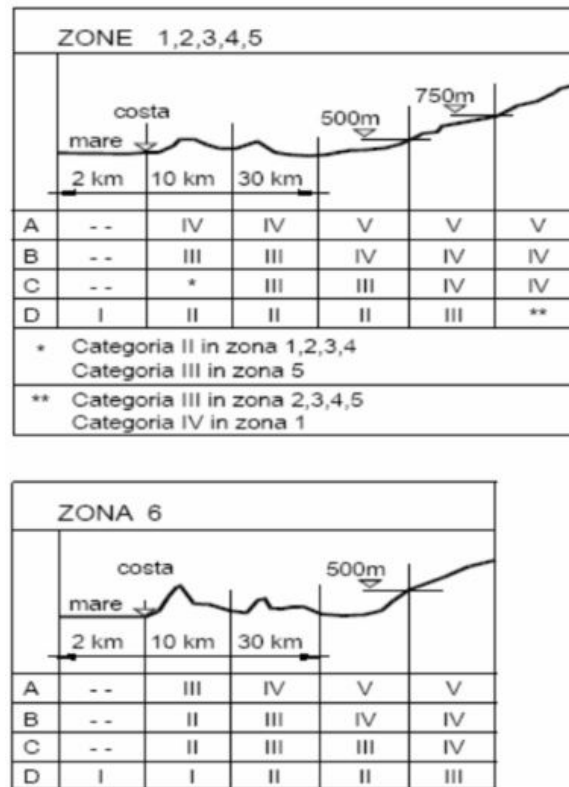


Figure 4.9: Parameters for the exposure coefficient definition

e) Force Coefficient

Considering that the structure under analysis is a bridge is mandatory to consider two cases: the loaded case, in which it is considered the passage of traffic, and the unloaded case, in which the traffic is not considered. The main difference between the two cases is the final value for the total height of calculation:

Total Height of Calculation			
Quantity		Loaded Case	Unloaded Case
Height from the ground	$z[m]$	28.00	28.00
Height deck and pavement	$z_{imp}[m]$	3.35	3.35
Height of the moving loads	$z_{traff}[m]$	3.00	0
Height of the traffic barrier	$z_{barr}[m]$	2.50	2.50
Total height of calculation	$z_{tot}[m]$	34.35	33.85

Table 4.4: Total Height of Calculation

as is possible to notice in the loaded case it is taken the higher value between the traffic height and the barrier height, while in the unloaded case since the road traffic is not considered the height of the moving load is posed equally to zero. At this point, it is possible to define the force coefficient c_f , which takes into account the area affected by the action of the wind. The UNI EN 1991-1-4 gives graphs to determine the value of this coefficient:

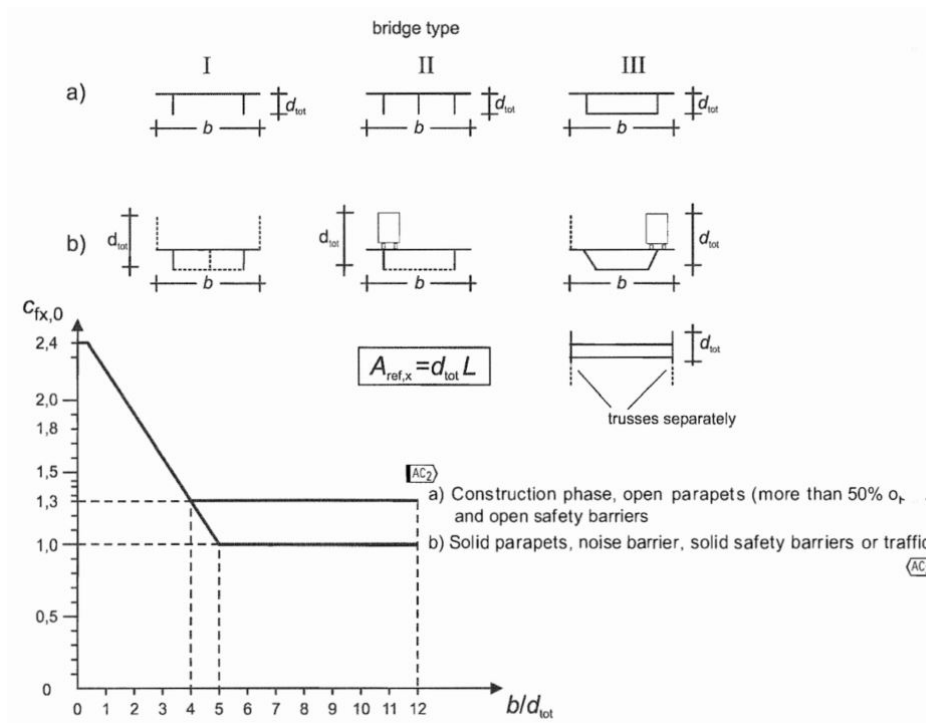


Figure 4.10: Force Coefficient

f) Wind Pressure and Wind Force At this point all the needed parameter and coefficient are known to obtain the wind pressure:

$$p = q_r \cdot c_e \cdot c_f \cdot c_d \quad (4.10)$$

in which q_r is the reference kinetic pressure, c_e is the exposure coefficient from, c_f is the force coefficient and c_d is the dynamic coefficient, it takes into account the reductive effects due to the non-contemporaneity of the maximum local pressures in addition with the amplifying effects of the dynamic response of the structure. The dynamic coefficient

can be assumed equal to 1 for safety reasons. [49]

Having the value of the wind pressure it is possible to finally obtain the wind force:

$$F_w = p \cdot d \quad (4.11)$$

in which d is the total reference height equal to the sum between the height of the deck and the maximum value between the height of the traffic barrier (z_{barr}) and the height of the moving load (z_{traff}). The numerical values used for the calculation and the final results are reported in the table above:

Wind Load Results			
Quantity		Loaded Case	Unloaded Case
Reference Base Velocity	$v_b [m/s]$	28.00	28.00
Reference Velocity	$v_r [m/s]$	28.00	28.00
Reference Kinetic Pressure	$q_r [KN/m^2]$	0.490	0.490
Exposure Coefficient	c_e	2.69	2.68
Force Coefficient	c_f	1.89	1.84
Total Reference Height	$d [m]$	6.35	5.85
Wind Pressure	$p [KN/m^2]$	2.50	2.42
Wind Force	$F_w [KN/m]$	15.87	14.18

Table 4.5: Wind Load Results

4.1.1.4 Thermal Action

Thermal loads are environmental loads strictly related to the daily and seasonal temperature variation, the study of the response of bridges subjected to this kind of loads is very important since they influence the long-term response and the durability of the structure [3]. The temperature distribution in bridges is generally non-linear and it is influenced by several conditions and parameters such as material type, bridge type and orientation, and shading from neighbouring structures [5]. Particularly important for analysing the thermal loads is the geographical location of the site where the structure takes place, in fact, it affects the air temperature defined within a range $[T_{max}; T_{min}]$, in which the two limit values are defined as the maximum shade air temperature in summer and the minimum shade air temperature in winter respectively, considering a return period of 50 years [49]. The construction site belongs to Zone I, therefore the two boundary values are taken as:

$$T_{min} = -15 - 4 \cdot a_s / 1000 \approx -15^\circ C \quad (4.12)$$

$$T_{max} = 42 - 6 \cdot a_s / 1000 \approx 44^\circ C \quad (4.13)$$

The thermal action should be then specified defining the following quantities:

- a) A uniform temperature component ΔT_u .
- b) A linearly varying temperature component ΔT_M .

For what concerns the range of uniform bridge temperature component, it is defined as:

$$\Delta T_{N,con} = T_0 - T_{e,min} \quad (4.14)$$

$$\Delta T_{N,exp} = T_{e,max} - T_0 \quad (4.15)$$

where T_0 is the initial bridge temperature taken equal to $15^\circ C$, while $T_{e,con}$ and $T_{e,exp}$ are, respectively, the minimum and the maximum uniform bridge temperature component obtained

by entering in the graph below knowing the values of the minimum and maximum shade air temperature:

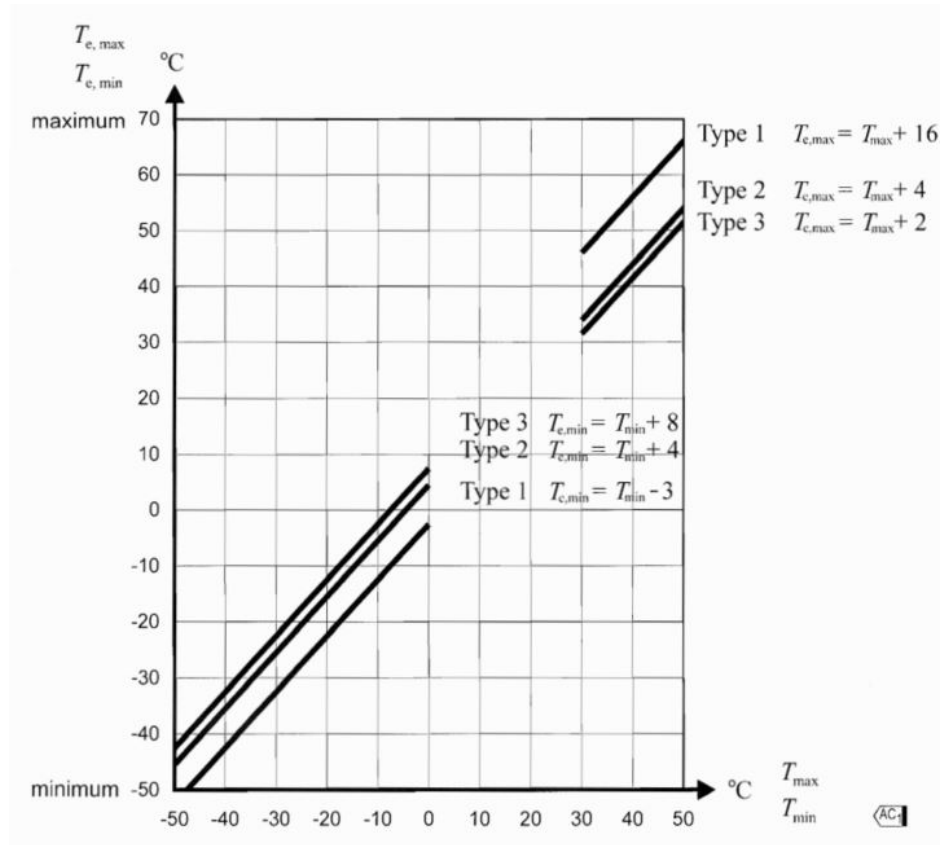


Figure 4.11: $T_{e,min}$ and $T_{e,max}$ recommended values

The choice of the correct straight line within the graph and, consequentially, of the correct formula to be used is given by the correct identification of the type of deck. The case study presents a deck type 3 (concrete deck with beams), therefore:

$$T_{e,max} = T_{max} + 2 \quad (4.16)$$

$$T_{e,min} = T_{min} + 8 \quad (4.17)$$

In addition to the uniform component, it is necessary to take into account the differential component, in fact considering a prescribed time period the heating and cooling process of the deck's upper surface will lead to a condition of maximum heating and maximum cooling

temperature variation [20]. The effect of these vertical temperature differences should be taken into account by defining a linear temperature difference component $\Delta T_{M,heat}$ and $\Delta T_{M,cool}$. These values have to be adjusted considering the effective surfacing thickness of the pavement by multiplying them for the coefficient k_{sur} :

Type of Deck	Top warmer than bottom	Bottom warmer than top
	$\Delta T_{M,heat}$ (°C)	$\Delta T_{M,cool}$ (°C)
Type 1: Steel deck	18	13
Type 2: Composite deck	15	18
Type 3: Concrete deck: - concrete box girder - concrete beam - concrete slab	10 15 15	5 8 8

NOTE 1: The values given in the table represent upper bound values of the linearly varying temperature difference component for representative sample of bridge geometries.

NOTE 2: The values given in the table are based on a depth of surfacing of 50 mm for road and railway bridges. For other depths of surfacing these values should be multiplied by the factor k_{sur} . Recommended values for the factor k_{sur} is given in Table 6.2.

Figure 4.12: Recommended values of linear temperature difference component

Road, foot and railway bridges						
Surface Thickness	Type 1		Type 2		Type 3	
	Top warmer than bottom	Bottom warmer than top	Top warmer than bottom	Bottom warmer than top	Top warmer than bottom	Bottom warmer than top
[mm]	k_{sur}	k_{sur}	k_{sur}	k_{sur}	k_{sur}	k_{sur}
unsurfaced	0,7	0,9	0,9	1,0	0,8	1,1
water-proofed ¹⁾	1,6	0,6	1,1	0,9	1,5	1,0
50	1,0	1,0	1,0	1,0	1,0	1,0
100	0,7	1,2	1,0	1,0	0,7	1,0
150	0,7	1,2	1,0	1,0	0,5	1,0
ballast (750 mm)	0,6	1,4	0,8	1,2	0,6	1,0

¹⁾ These values represent upper bound values for dark colour

Figure 4.13: Recommended values of k_{sur} to account for different surfacing thickness

The outcomes of the calculation previously explained are shown in the following table:

Thermal Load Results		
Quantity		Value
Minimum shade air temperature	$T_{min} [^{\circ}C]$	-15.0
Maximum shade air temperature	$T_{min} [^{\circ}C]$	42.0
Initial Temperature	$T_0 [^{\circ}C]$	15.0
Minimum uniform temperature component	$T_{e,min} [^{\circ}C]$	-7.0
Maximum uniform temperature component	$T_{e,max} [^{\circ}C]$	44.0
Maximum contraction range of the uniform component	$\Delta T_{N,con} [^{\circ}C]$	-22.0
Maximum expansion range of the uniform component	$\Delta T_{N,exp} [^{\circ}C]$	29.0
Heating equivalent linear temperature difference	$\Delta T_{M,heat} [^{\circ}C]$	10.5
Cooling equivalent linear temperature difference	$\Delta T_{M,cool} [^{\circ}C]$	-8.0

Table 4.6: Thermal Load Results

The simultaneously action on both uniform and differential component was considered by applying the following combinations:

$$\Delta T_{M,heat} (or \Delta T_{M,cool}) + w_N \cdot \Delta T_{N,exp} (or \Delta T_{N,con}) \quad (4.18)$$

$$w_M \cdot \Delta T_{M,heat} (or \Delta T_{M,cool}) + \Delta T_{N,exp} (or \Delta T_{M,con}) \quad (4.19)$$

where $w_N = 0.35$ and $w_M = 0.75$ are combination coefficients provided by the Eurocode.

4.1.1.5 Traffic Action

The structure of a bridge enables vehicles to overcome obstacles, but while doing so, they tend to generate internal stresses due to traffic-related static and dynamic movements. A single vehicle induces an action on a bridge structure, which splits into a quasi-static component depending upon the mass of the vehicle and a dynamic component mainly due to the vibrations of the vehicle that are a consequence of the pavement irregularities [40]. To perform the design of a bridge the European code defines imposed loads, models and representative values, associated with road traffic, including dynamic effects, centrifugal forces, braking and acceleration actions [45]. The traffic load models are mostly calibrated considering traffic surveys performed at high-loaded highways [18]. The main load models for vertical traffic loads provided by the Eurocode are described hereafter [20]:

- Load Model 1 (LM1):

The LM1 consider the combined application of axles and uniformly distributed loads and it is used to represent most of the effects of lorry traffic for general and local assessment [40], it is based on two subsystems: a system of concentrated axle loads named tandem system (TS) and a uniformly distributed loads system (UDL) [45]:

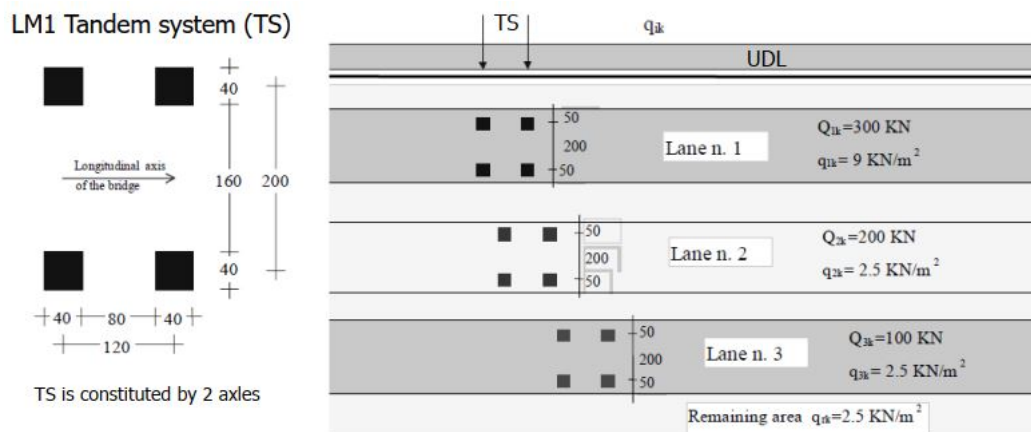


Figure 4.14: Load Model 1

- Load Model 2 (LM2):

The LM2 consider the application of a single axle load applied on a specific contact area, it is mainly used for local verification and to represent the effects of traffic on short structural members [35]:

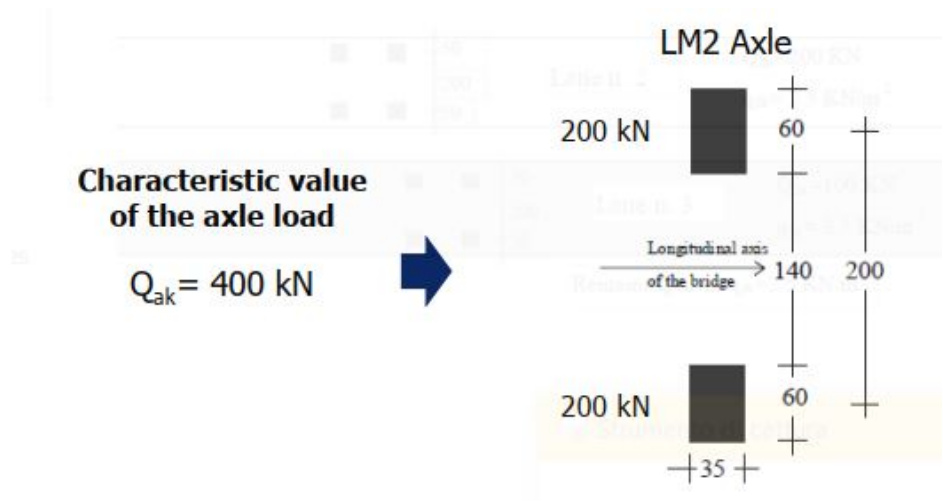


Figure 4.15: Load Model 2

- Load Model 3 (LM3):

The LM3 is intended for general and local verification, it considers the application of axle loads representing special vehicles [9].

The load models are applied on notional lanes having a width w_1 defined by the Eurocode:

Larghezza della superficie carrabile "w"	Numero di corsie convenzionali	Larghezza di una corsia convenzionale [m]	Larghezza della zona rimanente [m]
$w < 5,40 \text{ m}$	$n_l = 1$	3,00	$(w - 3,00)$
$5,4 \leq w < 6,0 \text{ m}$	$n_l = 2$	$w/2$	0
$6,0 \text{ m} \leq w$	$n_l = \text{Int}(w/3)$	3,00	$w - (3,00 \times n_l)$

Figure 4.16: Number and width of notional lanes

The arrangement of the notional lanes has to be determined in order to induce the most unfavourable condition of loading: considering that the carriageway has a total width of 11.25 m the total number of the notional lanes is 3 with a width w_1 taken equal to 3.00 m with a remaining area of 2.25 m width. A representation of the notional lanes is reported in the image below:

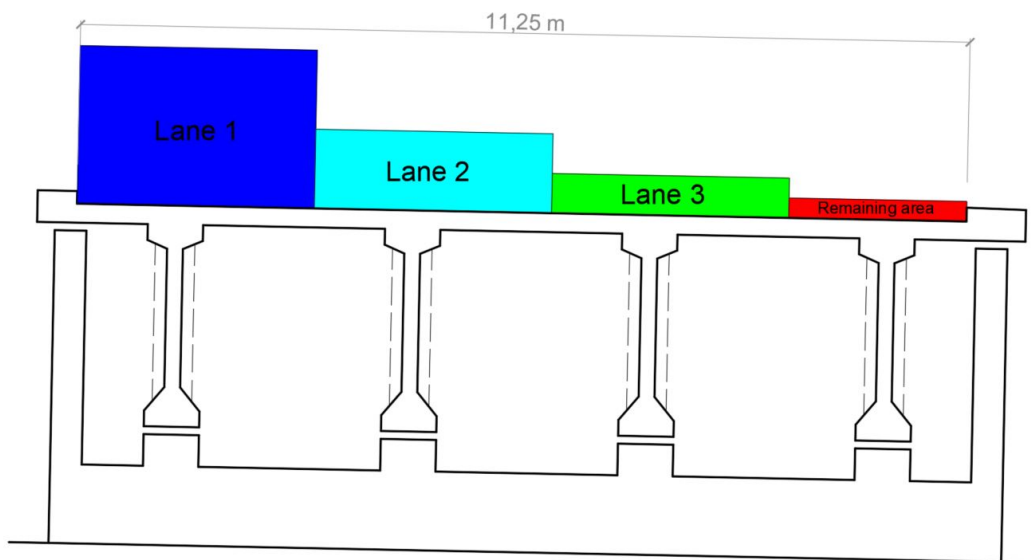


Figure 4.17: Notional lanes representation

Once defined the notional lanes configuration, it is possible to apply the Load Models. In this case study was applied the LM1 considering the following loads:

TS and UDL (LM1)		
Position	Axle Load (TS) - Q_{ik} [KN]	UDL - q_{ik} [KN/m ²]
Lane 1	300	9.00
Lane 2	200	2.50
Lane 3	100	2.50
Remaining Area	0	2.50

Table 4.7: TS and UDL values for LM1

In addition to the vertical loads represented by the LM1, it has to be considered the centrifugal force action and the longitudinal action of braking and acceleration, since the bridge under analysis has no curvature, only the braking and acceleration were taken into

account. The braking and acceleration force q_3 is a function of the vertical applied traffic load acting on the notional lane 1 and is defined as follows:

$$180KN \leq q_3 = 0.6 \cdot (2 \cdot Q_{1k}) + 0.10 \cdot q_{1k} \cdot w_1 \cdot L \leq 900KN \quad (4.20)$$

in which w_1 is the notional lane 1 width and L is the loaded length, in this case equal to 41 m, the calculated value for q_3 is then:

$$q_3 = 11.48 \text{ KN/m}$$

4.1.1.6 Load Combinations

To perform the assessment of the structure all the load combinations of the Ultimate Limit State (ULS) were conducted out, taking into account all the imposed loads previously described along with the appropriate combination factors specified by the code rules for the worst case scenario:

		Coefficiente	EQU ⁽¹⁾	A1	A2
Azioni permanenti g_1 e g_3	favorevoli sfavorevoli	γ_{G1} e γ_{G3}	0,90 1,10	1,00 1,35	1,00 1,00
Azioni permanenti non strutturali ⁽²⁾ g_2	favorevoli sfavorevoli	γ_{G2}	0,00 1,50	0,00 1,50	0,00 1,30
Azioni variabili da traffico	favorevoli sfavorevoli	γ_Q	0,00 1,35	0,00 1,35	0,00 1,15
Azioni variabili	favorevoli sfavorevoli	γ_{Qi}	0,00 1,50	0,00 1,50	0,00 1,30
Distorsioni e presollecitazioni di progetto	favorevoli sfavorevoli	γ_{e1}	0,90 1,00 ⁽³⁾	1,00 1,00 ⁽⁴⁾	1,00 1,00
Ritiro e viscosità, Cedimenti vincolari	favorevoli sfavorevoli	γ_{e2} , γ_{e3} , γ_{e4}	0,00 1,20	0,00 1,20	0,00 1,00

Figure 4.18: Partial Safety Factors for ULS Assessment

Azioni	Gruppo di azioni (Tab. 5.1.IV)	Coefficiente Ψ_0 di combi- nazione	Coefficiente Ψ_1 (valori frequent)	Coefficiente Ψ_2 (valori quasi permanenti)
Azioni da traffico (Tab. 5.1.IV)	Schema 1 (carichi tandem)	0,75	0,75	0,0
	Schemi 1, 5 e 6 (carichi distribuiti)	0,40	0,40	0,0
	Schemi 3 e 4 (carichi concentrati)	0,40	0,40	0,0
	Schema 2	0,0	0,75	0,0
	2	0,0	0,0	0,0
	3	0,0	0,0	0,0
	4 (folla)	--	0,75	0,0
	5	0,0	0,0	0,0
Vento	a ponte scarico SLU e SLE	0,6	0,2	0,0
	in esecuzione	0,8	0,0	0,0
	a ponte carico SLU e SLE	0,6	0,0	0,0
Neve	SLU e SLE	0,0	0,0	0,0
	in esecuzione	0,8	0,6	0,5
Temperatura	SLU e SLE	0,6	0,6	0,5

Figure 4.19: Combination coefficients for ULS Assessment

The performed combinations of actions applied on the model are reported in the table below, which highlights the used partial safety coefficients and the combination coefficients used for each load:

Loads Combinations								
Load	SLU (gr1)		SLU (gr2a)		SLU (Wind)		SLU (Temperature)	
	γ_{ij}	Ψ_{0i}	γ_{ij}	Ψ_{0i}	γ_{ij}	Ψ_{0i}	γ_{ij}	Ψ_{0i}
G1	1.35	-	1.35	-	1.35	-	1.35	-
G2	1.35	-	1.35	-	1.35	-	1.35	-
Traffic (TS)	1.35	-	1.35	0.75	1.35	0.75	1.35	0.75
Traffic (UDL)	1.35	-	1.35	0.40	1.35	0.40	1.35	0.40
Braking and Acc.	0	-	1.35	-	0	-	0	-
Wind	1.50	0.60	1.50	0.60	1.50	-	1.50	0.60
Temperature	1.35	-	1.35	-	1.35	-	1.35	-

Table 4.8: ULS Load Combination

4.1.2 Geometry

During the definition of the finite element model, it was selected to analyse only the central span between the two piers having a total length equal to 41 meters:

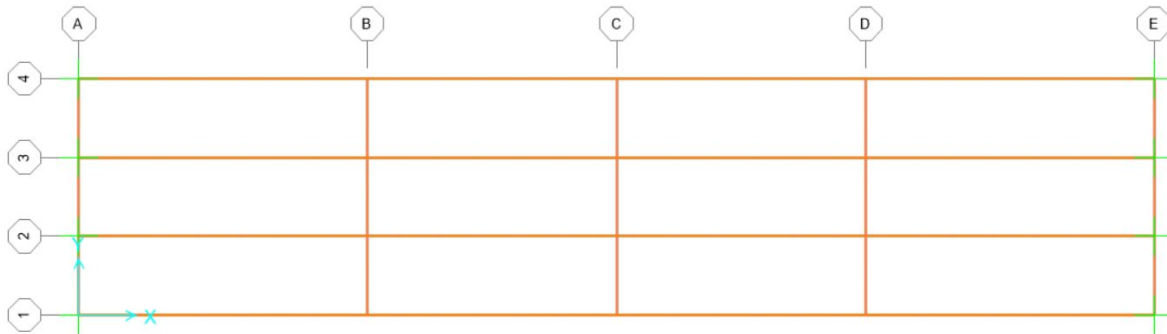


Figure 4.20: SAP2000 Model Plan

The characteristics of the beam elements in terms of cross-section, dimensions and used materials are the same described in the Cap.3.

4.1.3 Boundary Conditions

The model used for the FEA is a grid model composed of linear beam elements, having 6 Degree of Freedom (DOF): 3 rotational and 3 translational, the concrete slab was considered as part of the complex cross-section of beams and cross-beams considering the effective width calculated before. The piers were not modelled, while the bearings were defined as local restrains:

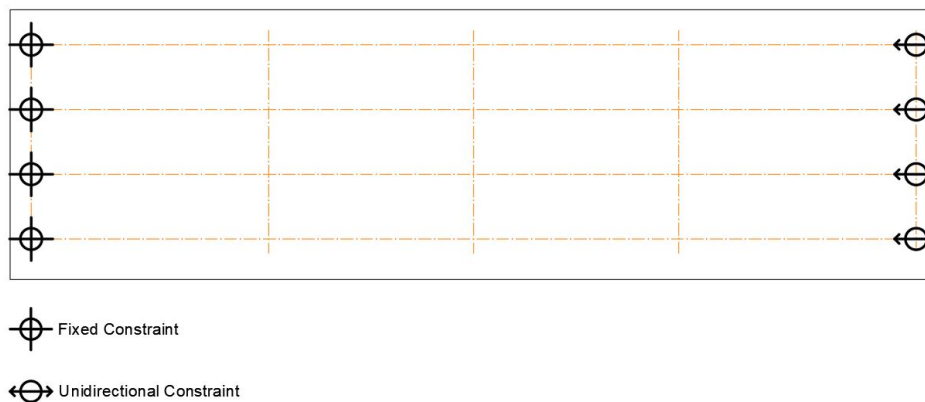


Figure 4.21: Restraints Configuration

4.2 Model Validation

The validation of the model was performed referring to the maximum bending moment of the main beam 2 (internal beam) due to the application of the permanent structural loads, non-permanent structural loads and traffic loads as indicated in the original documents of the bridge:

- Permanent structural loads:

The maximum bending moment acting on the main beam 1 reported in the original documents is the result of the application of a distributed load, which considers the sum of the self-weight of the beam, the weight of the cross-beams and the weight of the concrete slab;

- Permanent non-structural loads:

For the permanent non-structural loads the technical report provided a maximum bending moment that considers the application of a distributed load, which represents the self-weight of the concrete pavement;

- Traffic Loads:

The definition of the traffic loads acting on the bridge reported on the technical report is related to the standard in force at that time [11]. It splits the roads into two categories: roads intended for the transit of civilian and military vehicles and roads intended only for the transit of civilian vehicles. In addition, the standard proposed six traffic loads schemes defined as follows:

- Scheme 1: undefined column of lorries having a self-weight of 12 tons;
- Scheme 2: single road roller of 18 tons;
- Scheme 3: compacted crowd defined as a $400 \text{ Kg}/\text{m}^2$ areal load;
- Scheme 4: undefined column of military vehicles of 61.5 tons each;
- Scheme 5: undefined column of military vehicles of 32 tons each;
- Scheme 6: single military vehicle of 74.5 tons.

The case study is defined as a category 1 road, therefore it was loaded with a military vehicle scheme 5 and a civilian vehicle scheme 1:

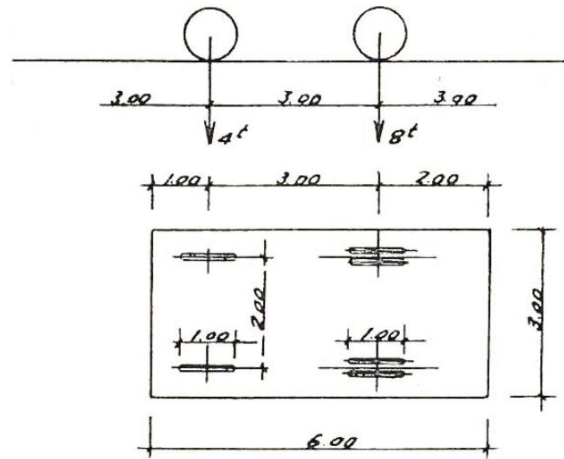


Figure 4.22: Scheme 1 - C.M. LL.PP. n. 384, 1962

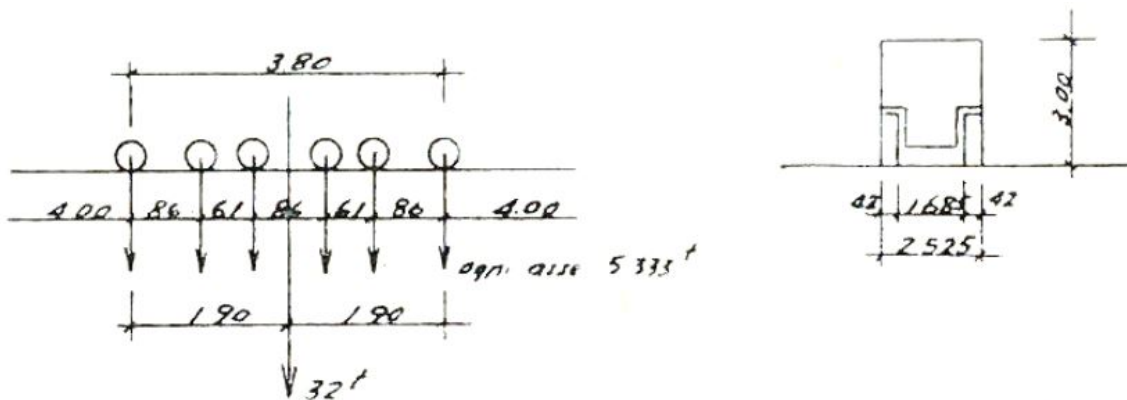


Figure 4.23: Scheme 5 - C.M. LL.PP. n. 384, 1962

The standard allowed to consider the application of the schemes described above as equivalent distributed loads depending upon the considered total length. Therefore the equivalent applied loads are:

$$Q_{c_{scheme1}} = 2.019 \text{ t/m} \approx 20.19 \text{ KN/m}$$

$$Q_{m_{scheme5}} = 4.155 \text{ t/m} \approx 41.55 \text{ KN/m}$$

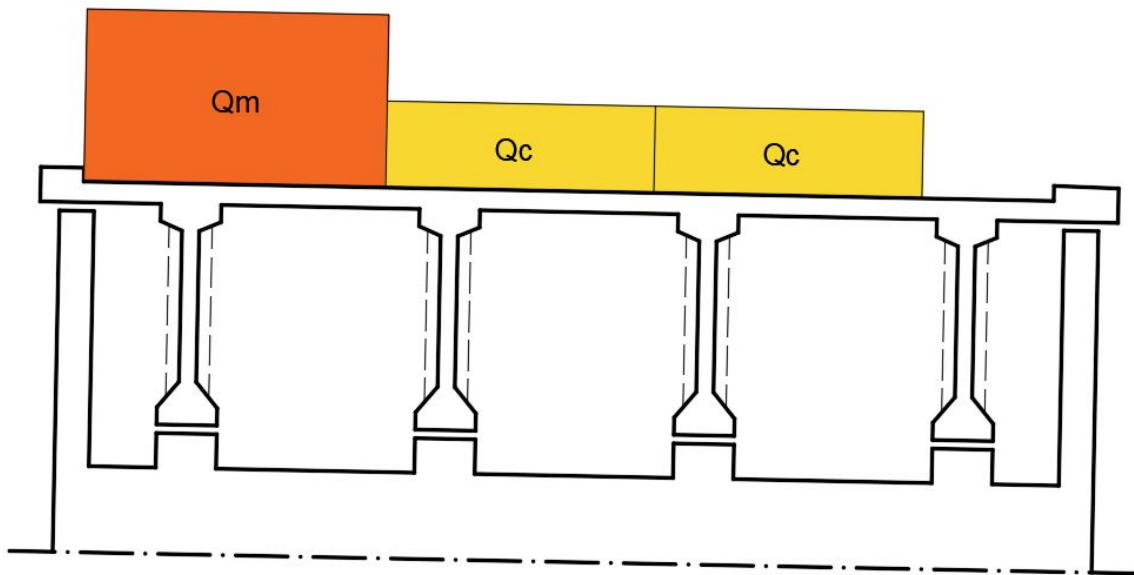


Figure 4.24: Scheme 1 and Scheme 5 application

To validate the FE model the same loads were applied and the maximum bending moment obtained in the three cases was compared with the values given in the technical report:

Model Validation Results					
Load Case	z [m]	M_{max} (FEM) [KN/m]	M_{max} (As Built) [KN/m]	ΔM [KN/m]	Err [%]
G1	20.5	8807.80	8857.40	49.60	0.56
G2	20.50	1455.71	1477.18	21.47	1.47
Traffic	20.50	6629.32	6935.99	306.67	4.6

Table 4.9: Model Validation

Having that in all of the three cases the error is less than 5% the validation of the model is considered successful.

4.3 Loads Transverse Distribution Analysis Results

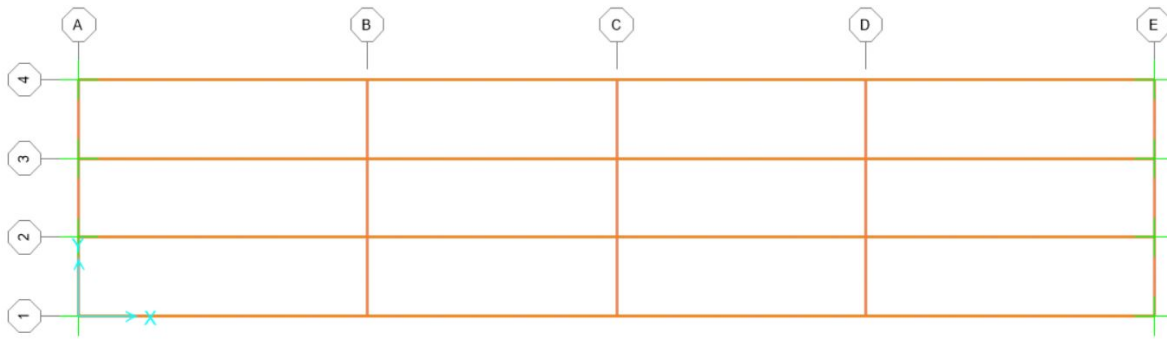


Figure 4.25: SAP2000 Model Plan

In the following pages the results in terms of bending moment diagram of the cross-beams (B, C, D) and the main beams (1 and 2) are reported taking as reference the fig. (4.25) and considering the loads combination defined in table (4.8):

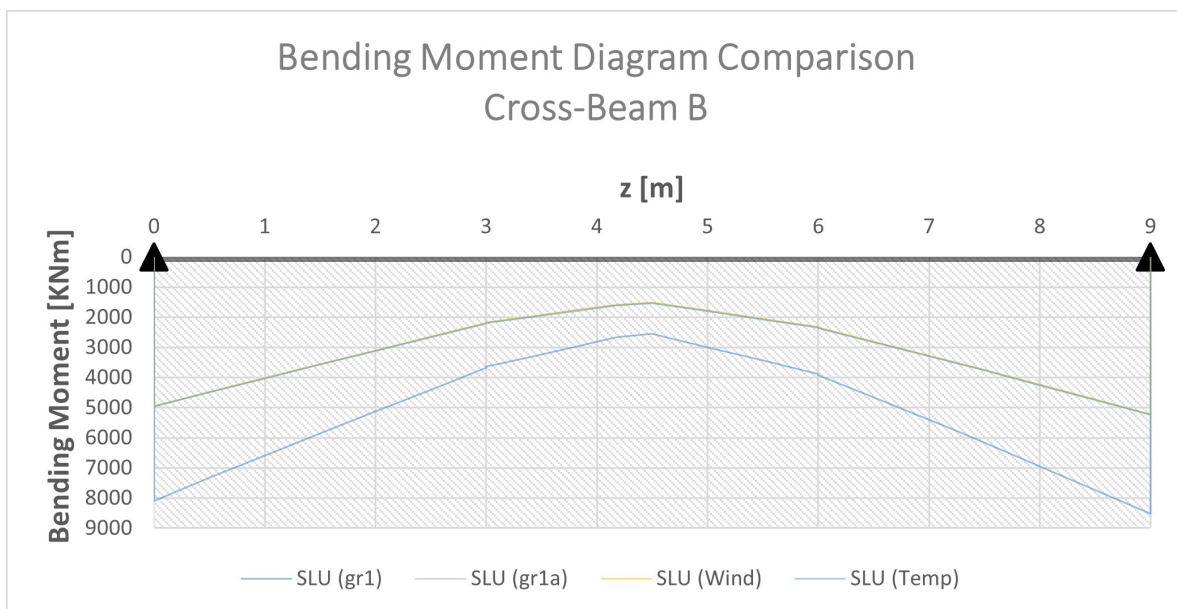


Figure 4.26: Bending Moment Diagram - Cross-Beam B

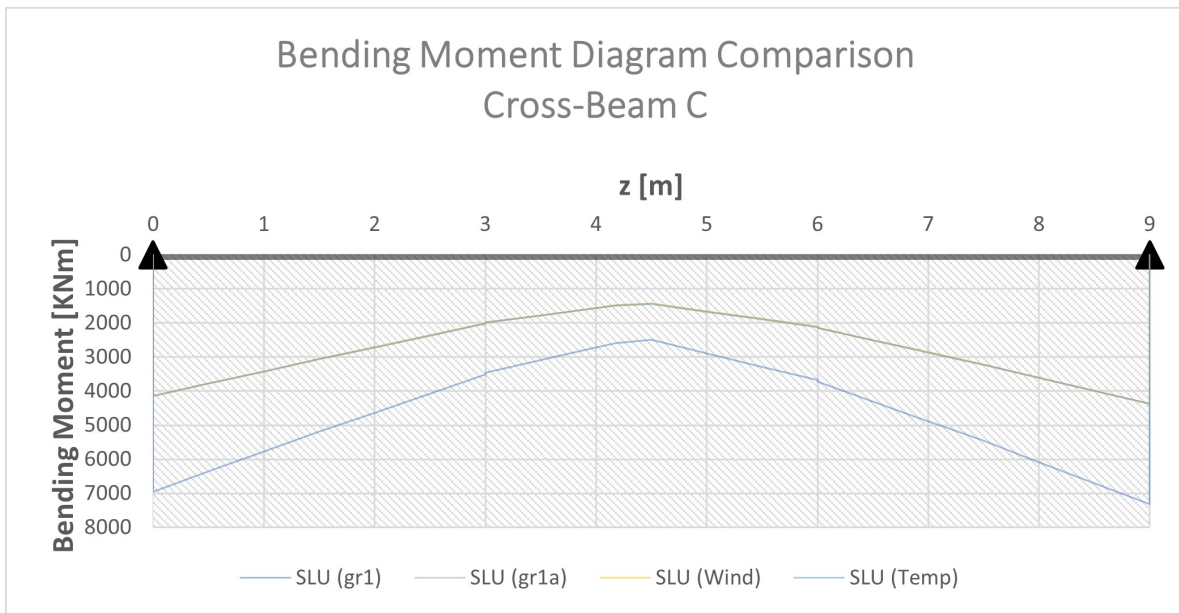


Figure 4.27: Bending Moment Diagram - Cross-Beam C

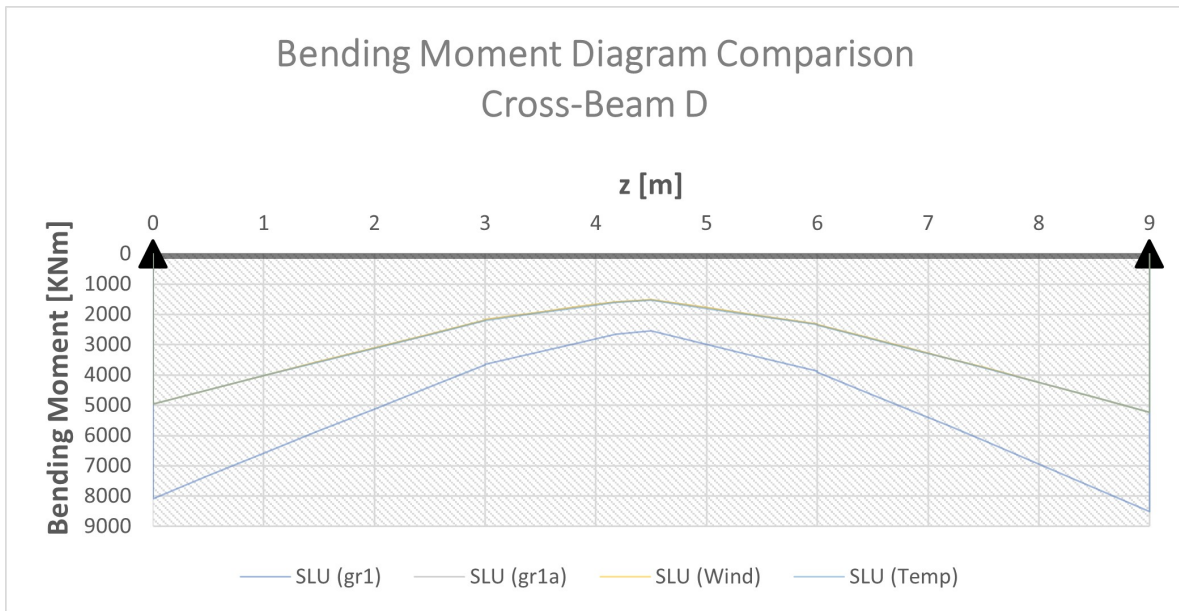


Figure 4.28: Bending Moment Diagram - Cross-Beam D

As can be seen, the cross-beams largest bending moments are applied at their edges, in correspondence with the connection to the edge main beams 1 and 4. This is compatible with the fact that the majority of the loads are applied to the edge main beams, which are more loaded than the two internal main beams. The main beams 1 and 2 bending moments, which

are shown below, support this idea:

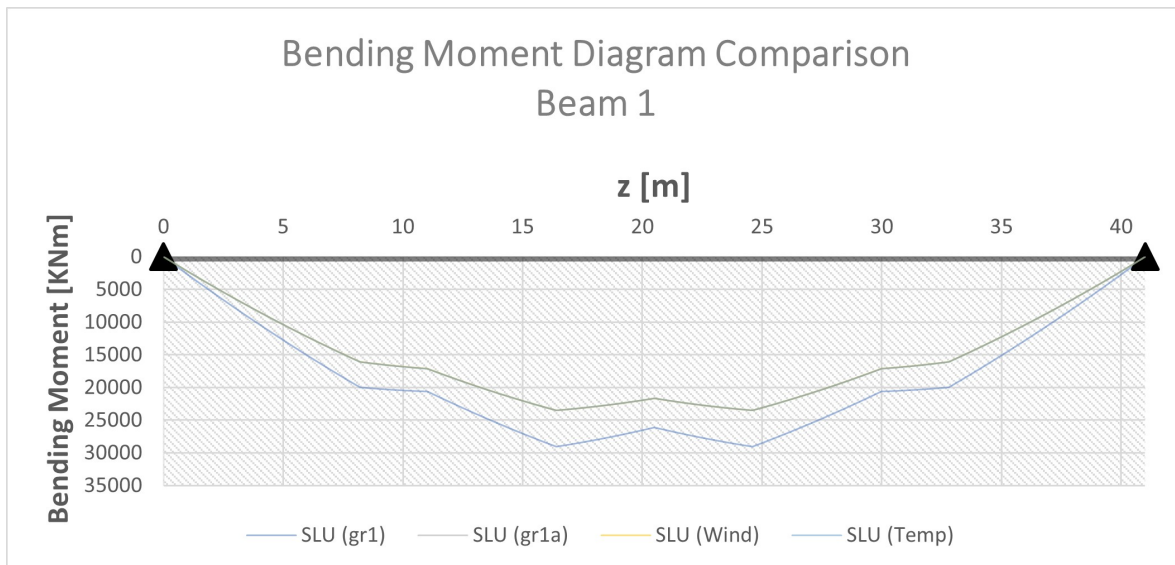


Figure 4.29: Bending Moment Diagram - Main Beam 1

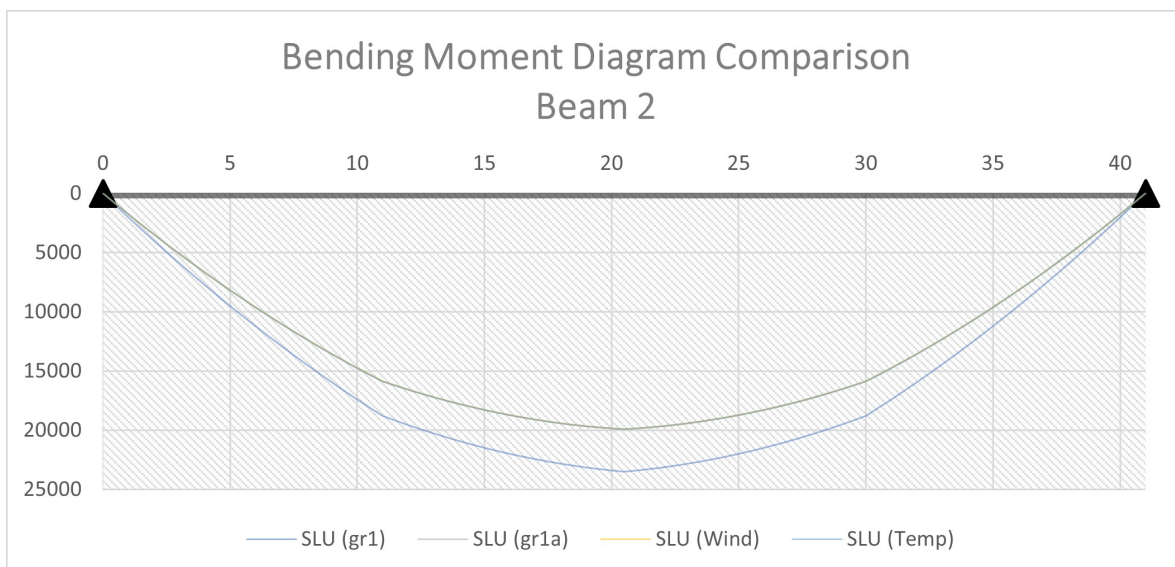


Figure 4.30: Bending Moment Diagram - Main Beam 2

As is possible to notice in fig. (4.29) the edge main beam 1 is more loaded than the internal main beam 2, moreover, it is possible to see how the diagram is subjected to a reduction of the bending moment value in correspondence of the cross-beams: at $z = 11$ m, $z = 20.5$ m and $z = 30$ m.

The following pages aim to study the influence of the cross-beams in terms of the maximum bending moment applied on the main beams, to do that firstly a comparison between the original FE model and a new model, in which the cross-beams are not considered, was performed based on the most severe load combination, the SLU (gr1):

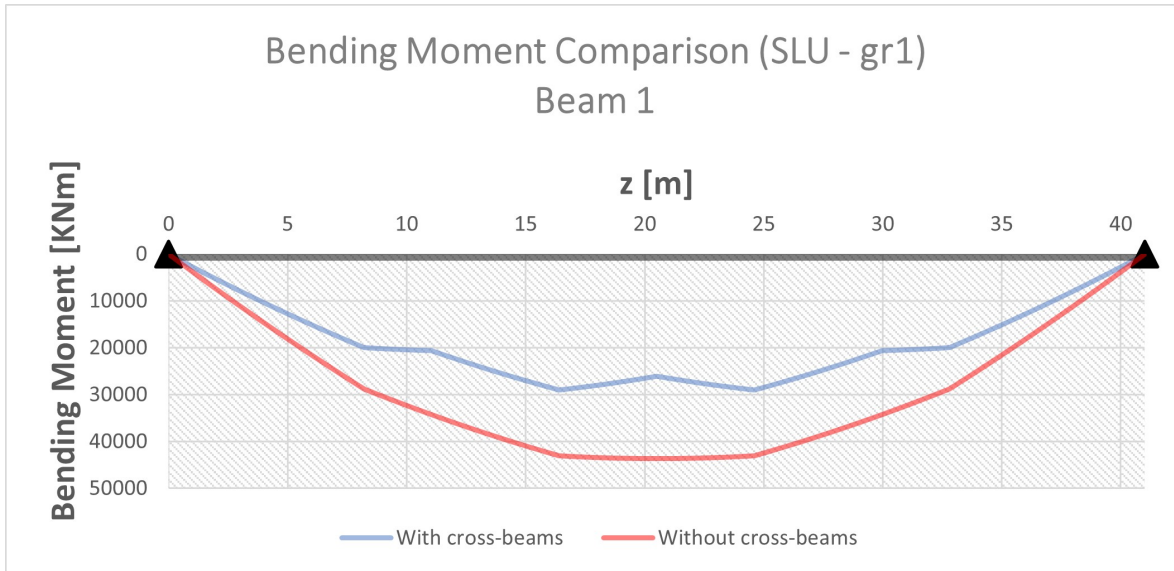


Figure 4.31: Bending Moment Diagram Comparison - Main Beam 1

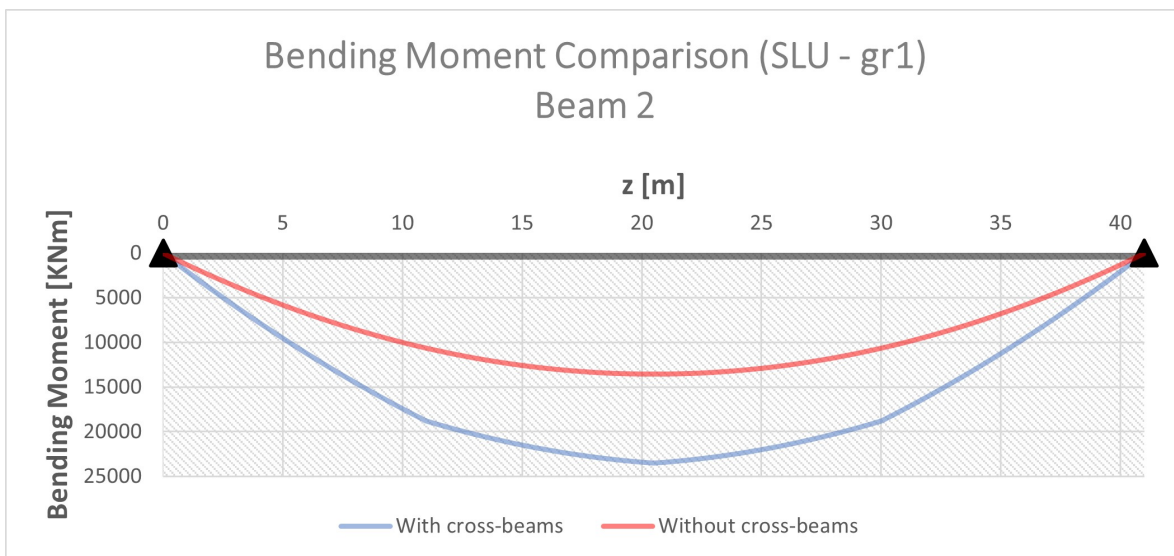


Figure 4.32: Bending Moment Diagram Comparison - Main Beam 2

The two diagrams confirm the expected behaviour: beam 1 (edge beam) results more loaded in the model without the cross-beams, while beam 2 (internal beam) has the opposite

attitude. Moreover, there is a relevant difference between the maximum bending moment acting on the edge beam and the one acting on the internal beam, this is mainly since the main beams are more stressed by the combined action of traffic and wind loads in the SLU (gr1) loads combination than the internal beams. In addition of that, from fig. (4.31) and fig. (4.32) it is possible to notice that the absence of the cross-beams induces an increase in bending of the edge beams, while it reduces the applied bending moment on the internal main beam. These results are consistent with the fact that the cross-beams can be considered as elastic constraints applied on the main beams making them a hyperstatic structure:

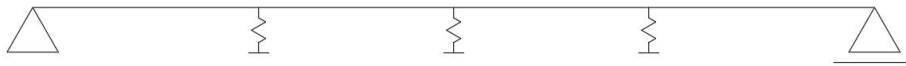


Figure 4.33: Main Beam simplified static scheme

At this stage, it proceeds with the study of the actual contribution of the cross-beams in terms of the transversal distribution of the loads referring to the moment difference between the edge and the internal main beam. Firstly a constant distributed load $q = 30 \text{ KN/m}$ was applied on each main beam:

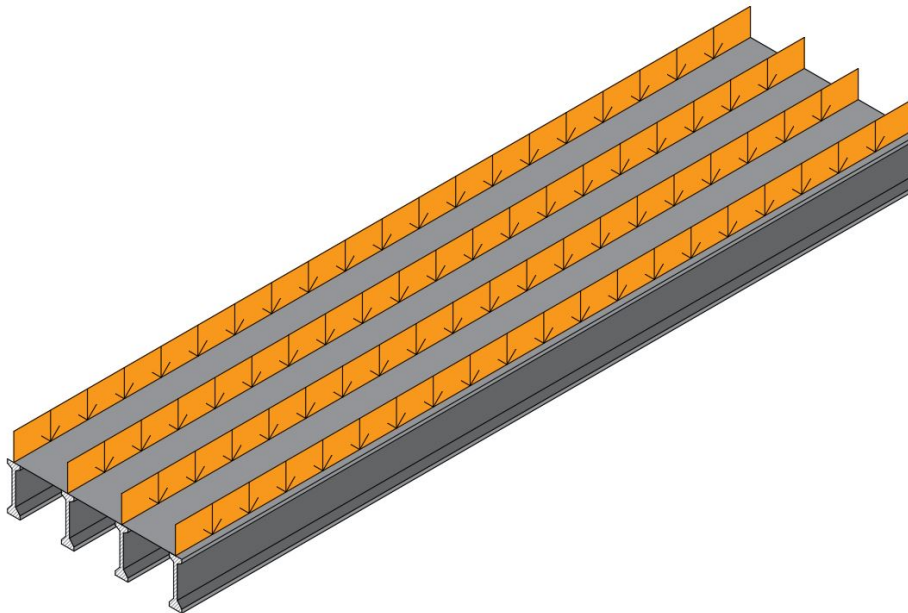


Figure 4.34: Loading case

The bending moment acting on the edge main beam and on the internal main beam was recorded, the mid-span cross-section was taken as a reference, and the difference between the two values was calculated (ΔM). To determine the actual contribution of the cross-beams in different configurations the (ΔM) was calculated by changing the total number of the cross-beams and consequently the distance between them:

(ΔM) Calculation				
n°Cross-Beams	i [m]	$M_{z=20.5m}$ (Beam 1) [KNm]	$M_{z=20.5m}$ (Beam 2) [KN/m]	ΔM [KN/m]
2	20.5	6387.85	6195.78	192.07
3	13.7	6397.22	6211.76	185.45
Case Study	variable	6396.90	6212.14	184.76
4	10.25	6391.37	6216.08	175.28
5	8.20	6395.49	6213.91	181.58
6	6.83	6393.19	6216.16	177.03
7	5.86	6395.16	6214.76	180.39
8	5.125	6393.78	6215.96	177.82
9	4.56	6395.08	6215.17	179.92
10	4.1	6394.23	6215.95	178.28

Table 4.10: ΔM calculation

The variation of the moment increment (ΔM) with the change of the number of the cross-beams is represented in the graph below:

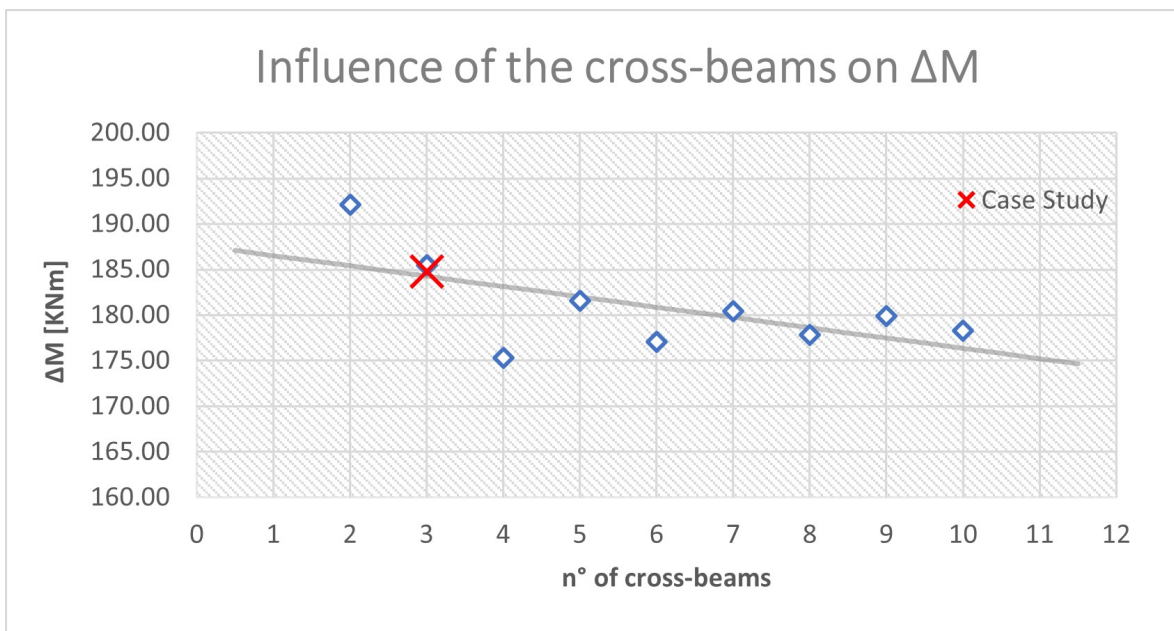


Figure 4.35: Influence of the cross-beams on ΔM

From fig. (4.35) it is possible to deduce several things:

- The difference (ΔM) between the bending moment acting on the edge main beam and the bending moment acting on the internal beam tends to decrease with the increase of the number of cross-beams. This result is consistent with the fact that one of the consequences of the cross-beams increase is that the two beams become more integrated, increasing the efficiency of the transverse distribution of the loads.
- Although the increase of the number of cross-beams tends to decrease ΔM , it is possible to notice that exceeding the number of six cross-beams the variation of ΔM is very limited. This result is consistent considering that increasing too much the number of cross-beams leads to an oversizing of the structure.
- As expected the worst configuration in terms of (ΔM) is the one with 2 cross-beams, while the best configuration is the one with 4 cross-beams.

The results above were obtained taking as the main variable the number of cross-beams, and consequently the distance between them, leaving unchanged other parameters that can influence the transversal load distribution like the torsional rigidity of the main beams or the flexural rigidity of the cross-beams.

CHAPTER

5

Fatigue Analysis

The aim of the following chapter is to give an overview of the fatigue phenomenon and in particular the fatigue on concrete under compression. Then a study about the influence of the cross-beams on the behaviour of the structure case study subjected to fatigue loads is presented.

5.1 Introduction to the Fatigue Phenomenon

Among many definitions of the term fatigue, the one proposed by the American Society for Testing Materials (ASTM) cites: "Fatigue is a permanent, progressive and localized process of structural change in a material subjected to time-varying stress and strain conditions which can lead to cracking and/or fracture after a sufficient number of cycles"[1]. This definition allows to define several peculiarities of the fatigue phenomenon:

- Permanent: in other words it is not reversible;
- Progressive: each application of the loads induces damage, which can be accumulated;
- Localized: it is not a phenomenon of degradation of the characteristics of the whole material but it affects a limited portion of a structural element.

Moreover, the fundamental concept related to the fatigue phenomenon of a structural component is that it is characterized by a deterioration that occurs as a consequence of a cyclic

repetition of loads that individually applied cannot produce failure [25], one of the indicators of fatigue damaging is the reduction of the elastic modulus [28]. To define a loading cycle at least two parameters related to the stresses[33]:

- Maximum stress σ_{max} ;
- Minimum stress σ_{min} ;
- Mean stress $\sigma_m = \frac{\sigma_{max} + \sigma_{min}}{2}$;
- Alternating stress $\sigma_a = \frac{\sigma_{max} - \sigma_{min}}{2}$;
- Stress amplitude $\Delta\sigma = \sigma_{max} - \sigma_{min}$;
- Fatigue ratio $R = \frac{\sigma_{min}}{\sigma_{max}}$;
- Amplitude ratio $R_a = \sigma_a \cdot \sigma_m$.

To fully define a cyclic stress history at least two of the above parameters are needed.

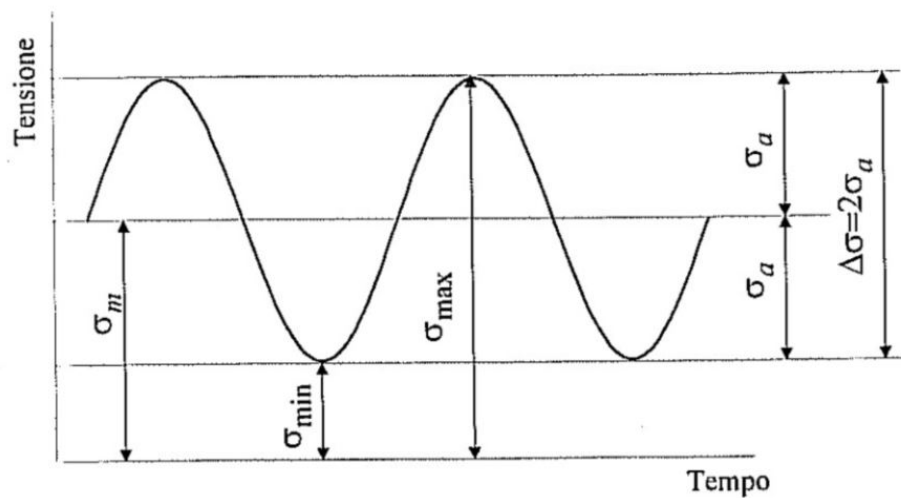


Figure 5.1: Fatigue stress cycle

Typical cyclic loads are wind, waves, traffic loads and vibrations, these loads mainly affect structures such as bridges, skyscrapers and offshore structures. Cyclic loads are divided into two different categories: low-cycle fatigue (up to 10^6 cycles) and high-cycle fatigue (between $10^3 - 10^7$ cycles):

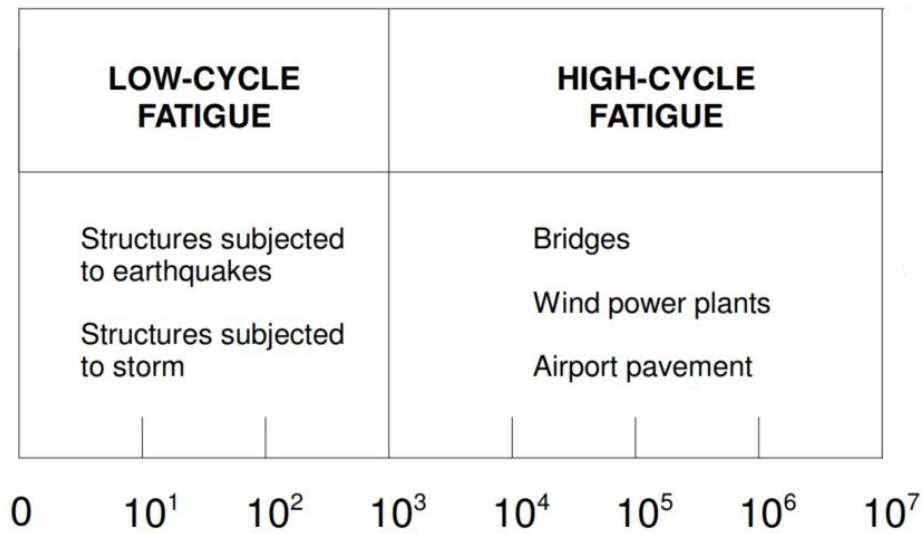


Figure 5.2: Spectra of fatigue load categories [19]

5.1.1 Microscopic aspects of fatigue

From a microscopic point of view, a fracture due to the fatigue phenomenon takes place following three phases:

- Nucleation phase:

The cracks due to fatigue generally start from the material surface. If the applied load is oriented parallel to the plane containing the superficial grains, the dislocation movement induces a sliding between the crystalline planes [6].

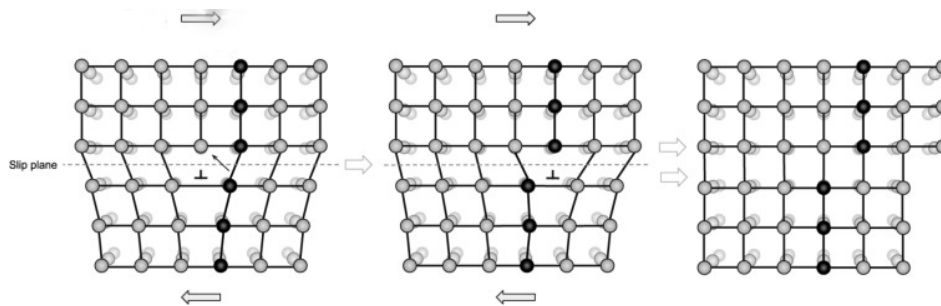


Figure 5.3: Dislocation movement

After its formation, the slip band emerge at the surface generating intrusions and extrusions, which induces a stress concentration where fatigue cracks nucleate [21]. The movement of an atom from its original position in the crystalline scheme is permanent and not reversible, therefore it leads to plastic deformations at the microscopic level.

- Propagation phase:

As the cyclic stress proceeds, the micro-cracks tend to unite, generating a macro-crack that begins to propagate in the direction normal to the orientation of the applied load. At this point, the development of the phenomenon is related to material strength.

- Collapse phase:

When the crack size reaches the critical value, fracture of the piece occurs; this fracture may occur in a brittle manner or by plastic collapse; in the great majority of cases, fracture occurs in a brittle manner without any apparent permanent deformation. Crack growth leads to a progressive decrease in the resistant section: when this becomes so small that it is no longer able to resist external stresses, the final crash fracture occurs due to static overloading.

This process is well defined and known for steel, but since concrete and steel behave differently regarding fatigue, reinforced concrete is considered as the sum of two separate materials [24]. Concrete is not a homogeneous material, and when it hardens, pores and microscopic cracks appear. Furthermore, macro cracks frequently occur prior to the application of any stress because of shrinkage and temperature variations. Concrete can be thought of as a strain-softening material as a result of the cracks and inhomogeneity [19]:

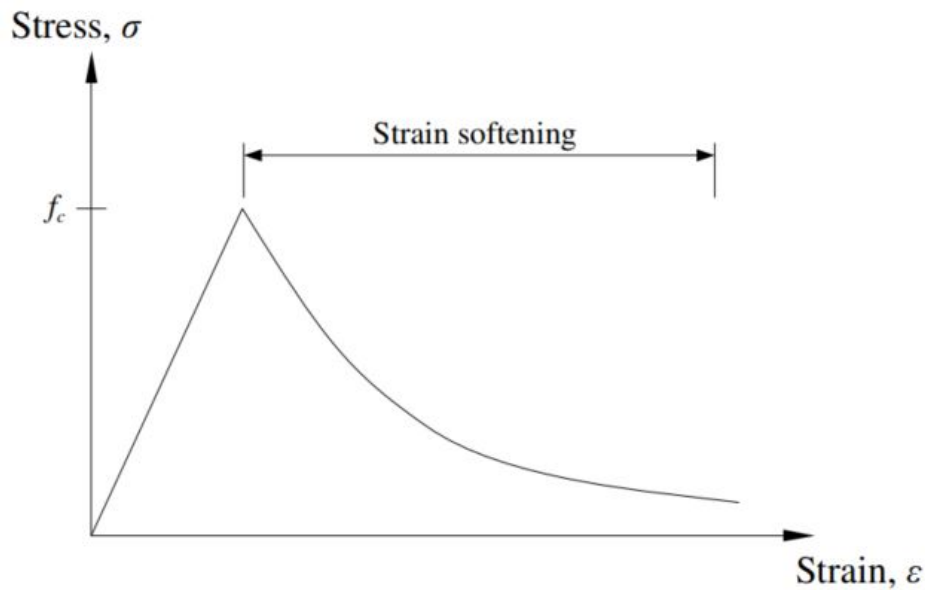


Figure 5.4: Decreasing stiffness of concrete due to strain softening

Since cracks already exist, there won't be a distinct crack initiation process when the concrete is subjected to cyclic stress. Instead, these cracks will advance gradually at first, then more quickly, until the remaining portion of the concrete section fails [7].

5.1.2 Fatigue in reinforced concrete members

As far as reinforced concrete is concerned, being a composite material, its fatigue behaviour varies depending on the element considered:

- Concrete:

Under force-controlled compression or tension fatigue loading, plain concrete shows substantially growing stresses during the initial phase of life, which is followed by a phase of stable, but barely increasing strains. During this final time, the concrete matrix experiences severe micro-cracks caused by uniaxial compression. Following the failure, an increasing number of cracks on the outer surface appear parallel to the direction of loading. The early-age micro-cracks in the cement matrix and at the interface between aggregates and the cement matrix propagate steadily and perpendicular to the loading direction until the specimen fractures show one discrete crack. Crack propagation also

dominates concrete behaviour under tension fatigue loading[16] [13].

- Steel reinforcement:

A steady crack propagation phase, brittle fracture of the remaining portion, and a crack starting phase can be used to categorise the fatigue life of steel reinforcement. The root of a rib is typically where a crack in a high-yield steel bar with ribs originates, which creates stress concentration. Low fatigue strength is caused by welds, bent bars' curvature, and corrosion, which all favour the development of cracks [37].

- Reinforced concrete members:

The bond between reinforcement and concrete gradually deteriorates due to fatigue loading. Greater deflection is caused by wider cracks and less concrete filling in the tension between the cracks. Rebars fatigue fracture is the typical cause of failure; concrete spalling in the compression zone is another failure mechanism[42].

5.1.3 Fatigue analysis methods

The final goal of a fatigue study is often to calculate the fatigue life of a structure, which can be done by counting the number of fatigue load cycles or the amount of damage that a construction detail can withstand before failing. There are several ways to perform a fatigue analysis, including:

- Fracture mechanics:

Fracture mechanics techniques that introduce a softening crack, i.e. the stress transfer reduces with increasing crack opening are utilised to prevent fatigue crack propagation in concrete. Tensile tests have been suggested and numerically simulated, and several models for the cracking behaviour of plain concrete under cyclic loading have also been proposed;

- Damage accumulation:

Models for damage accumulation make it possible to gauge the extent of harm brought on by various pressures. The linear damage accumulation by Palmgren-Miner is the most popular theory. It is based on S-N curves and describes the total damage resulting from each of the individual cycles applying the Palmgren-Miner cycle ratio summation, which predicts the failure of the component when:

$$D = \sum_{i=1} \frac{n_i}{N_i} = 1 \quad (5.1)$$

where, for a given load amplitude or cyclic stress, n_i is the applied number of cycles and N_i is the number of cycles at which failure occurs [50]. The Palmgren-Miner Rule is highly erroneous when applied to gross cycles with few load changes since it does not account for prior stress history or the pattern of loading [26];

- S-N curves approach:

S-N curves are graphical representations of the relationship between cyclic stress range and the number of cycles to fatigue failure in a logarithmic scale. The most popular S-N curve for calculating fatigue life and estimating the accumulation of fatigue damage is the Wöhler curve. Usually, through the implementation of Experimental Stress Analysis and long-term fatigue tests with constant stress amplitude can the curve be derived [44]. For steel, the S-N curve approach is widely used, it is possible to find various curves within the standards and code rules. The Eurocode provides several S-N curves for steel construction details that express the number of cycles to failure as a function of stress variations in the cycle $\Delta\sigma$ or $\Delta\tau$ [38]. Unlike steel, knowledge of the fatigue behaviour of concrete is still limited. This has led over the years to a certain degree of uncertainty regarding the treatment of this phenomenon within the relevant standards [42], the Eurocode does not provide any kind of S-N curves for concrete. It should be emphasised that the maximum stress level allowed in a structure designed under serviceability condition is usually lower than the fatigue limit of concrete, which become sensitive to cyclic loading only above 60% of its static compressive strength [16].

5.2 Fatigue of concrete under compression

As already mentioned the fatigue analysis of concrete is still experimental and affected by a lack of knowledge. Moreover, in the case of the analysis of an existing bridge, some considerations must be made[42]:

- Cracks spread as a result of the deterioration of concrete and steel caused by fatigue. Many applications of fracture mechanics have been made in the field of steel structure fatigue. The importance of fracture mechanics in reinforced concrete is acknowledged, and there are promising methods for characterising the low cycle fatigue behaviour of concrete [22]. The development of models for high cycle fatigue of reinforced structural parts, specifically for shear failure. Thus, fracture mechanics is not yet applicable to concrete for the examination of existing bridges.
- An existing bridge's reliability index and cumulative fatigue damage could be estimated using a damage accumulation approach for concrete. It has been demonstrated that slender flexure members' concrete compression zone will not fail under fatigue stress. Because the fatigue damage process is unknown, there is no damage accumulation theory for the more significant situation of shear fatigue. Hence, the buildup of concrete damage still has no real-world use.
- The S-N technique produces straightforward values that indicate fatigue safety, but it does not explain the phenomena of fatigue or its effects. The offered detail categories for reinforcement should be updated and integrated with damage accumulation and reliability analysis for the inspection of existing bridges.

The Eurocode does not give any kind of S-N curves for concrete, but many studies over the years have proposed S-N curve models for the various concrete classes. To obtain those curves fatigue tests were performed on concrete specimens, which were loaded between a lower and an upper-stress limit. These limit values are expressed as fractions of the concrete compressive strength:

$$S_{max} = \frac{\sigma_{c,max}}{f_{ck}} \quad (5.2)$$

$$S_{min} = \frac{\sigma_{c,min}}{f_{ck}} \quad (5.3)$$

It is crucial to draw attention to the fact that fatigue cracking in concrete is more difficult to identify than fatigue cracks in other materials, such as steel. Nonetheless, it is evident that there are some conditions, which significantly influence the behaviour of the structure or elements under analysis [29]:

- Repetitive bending that causes secondary strains;
- Higher rolling loads and traffic pressures on slabs, pavements, and bridges that are more frequent or greater in magnitude;
- Dead load stresses are significantly less than live load stresses;
- Recurrent impact and other stresses on pavement joints, bridge bearings, and other structural components;
- Vibration, especially when associated with impurities and dynamically active components;
- Points where repetitive loads are applied, that are not sufficiently restricted;
- Chemical attacks, fretting, and pitting, especially in prestressed concrete;
- Carbonation attack, especially in reinforced concrete.

5.3 Influence of the transverse distribution of loads

In the following pages, the Finite Element Model is updated to analyse the influence of the cross-beams in resisting the fatigue phenomena and distribution of loads. As explained in chapter 4, cross-beams are structural elements whose main function is to allow the correct transfer of loads in the transverse direction. This function becomes fundamental in the case of the application of traffic load models, which are asymmetrical load configurations that lead to increased stress in the edge beams. In chapter 4 it was explained how the application of a symmetrical load configuration determines a difference in bending moment applied between the edge beam and the interior beam, at this point the intention is to determine the moment difference given by the application of fatigue-inducing loads in the structure.

5.3.1 Fatigue Load combination

As for the traffic load models, the Eurocode defines specific load models for fatigue [49]:

- Fatigue Load Model 1 (FLM1):

The FLM1 is similar to the LM1, it assumes 70% of axle loads and 30% of distributed loads, both applied on the conventional lanes defined as described in the chap.4:

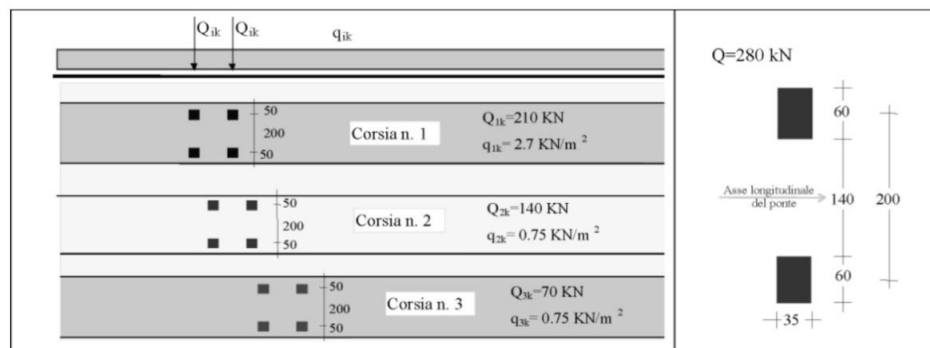


Figure 5.5: Fatigue Load Model 1

This model is extremely simple and conservative [15].

- Fatigue Load Model 2 (FLM2):

This model is used when more specific analyses are required. It does not consider the

effects of multiple loaded lanes, only the notional lane 1 is loaded by a set of lorries with frequent valued of axle loads:

Sagoma del veicolo	Distanza tra gli assi (m)	Carico frequente per asse (kN)	Tipo di ruota (Tab. 5.1.IX)
	4,50	90 190	A B
	4,20 1,30	80 140 140	A B B
	3,20 5,20 1,30 1,30	90 180 120 120 120	A B C C C
	3,40 6,00 1,80	90 190 140 140	A B B B
	4,80 3,60 4,40 1,30	90 180 120 110 110	A B C C C

Figure 5.6: Set of lorries for Fatigue Load Model 2

- Fatigue Load Model 3 (FLM3) and Fatigue Load Model 4 (FLM4):

These are models predominantly used for damage assessment using the Palmgren-Miners law.

The calculation of maximum and minimum applied stress values is obtained by applying the frequent combination of the loads that do not induce fatigue and the combination of the actions cause fatigue [20]:

$$\sum_{j \geq 1} G_{kj} + P + \psi_{11} \cdot Q_{k,1} + \sum_{j > 1} \psi_{2,i} \cdot Q_{k,1} \quad (5.4)$$

$$\sum_{j \geq 1} G_{kj} + P + \psi_{11} \cdot Q_{k,1} + \sum_{j > 1} \psi_{2,i} \cdot Q_{k,1} + Q_{fat} \quad (5.5)$$

5.3.2 Definition of Case 0 and Overloaded Case

The study aims to link the fatigue behaviour of concrete under compression and the transverse distribution of loads provided by the cross-beams. It was demonstrated before in this thesis how the presence of cross-beams determines a difference in the applied bending moment between the edge beam and the interior beam and how the absence of the cross-beams determines an increase in the bending moment applied to the edge beam. The objective of this phase is to design an overload that reflects the level of hyperstaticity provided by the presence of the cross-beams. This is accomplished by applying the fatigue combination load expressed in eq.(5.5) to the structure by taking the FLM3 into account and recording the bending moment acting on the mid-span cross-section of the edge beam and interior beam. The difference between the two values is then calculated:

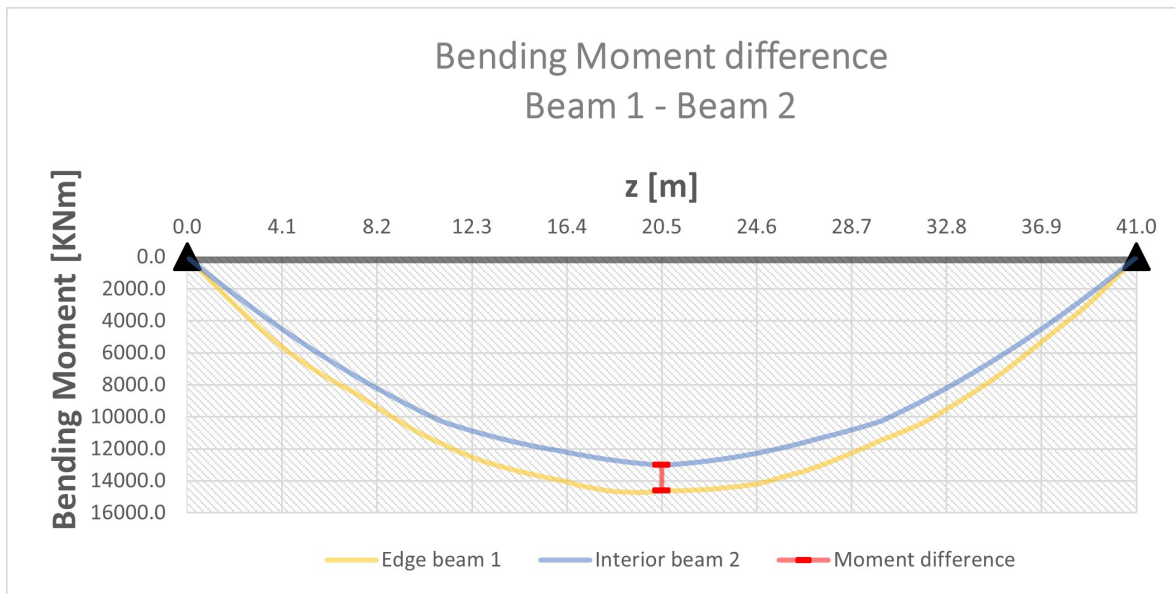


Figure 5.7: Bending moment difference between beam 1 and beam 2

z [m]	M_{Beam1} [KNm]	M_{Beam2} [KNm]	ΔM [KNm]
20.5	14620.70	13015.36	1605.34

Table 5.1: Value of the Bending moment difference for Case Study

The overload is then defined as the uniformly distributed load necessary for the simply supported (absence of cross-beams) internal beam to show a bending moment at the mid-span cross-section equal to ΔM :

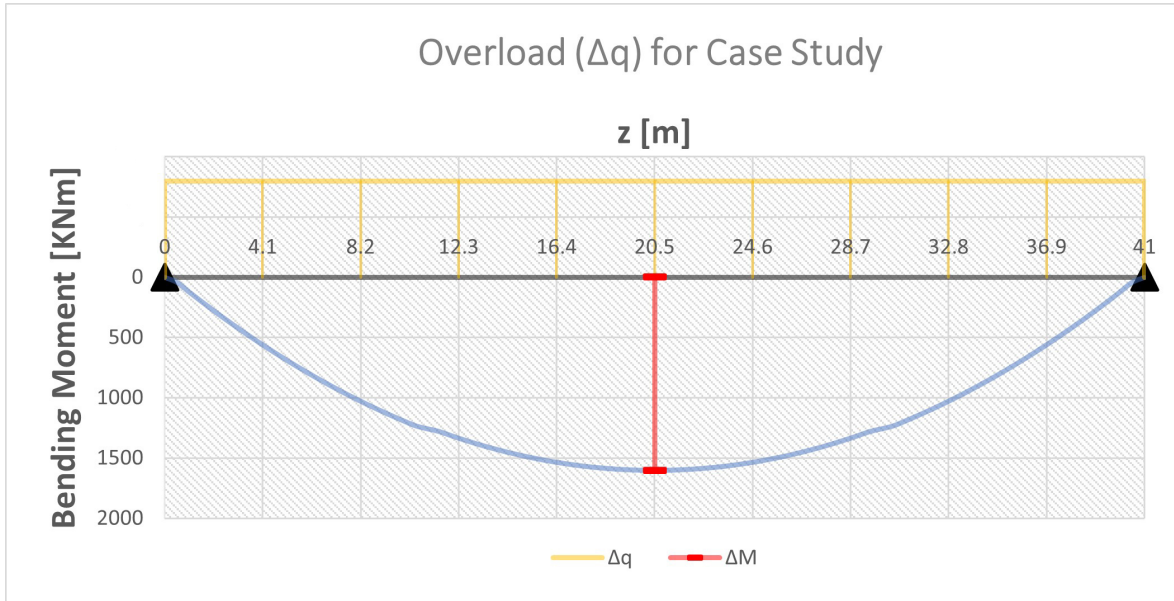


Figure 5.8: Overload for Case Study

All of the various cross-beam configurations of the model already shown in chapter 4 are analysed following this procedure and for each configuration, the value of the overload is determined:

Overload Calculation				
n° cross-beams	M_{Beam1} [KNm]	M_{Beam2} [KNm]	ΔM [KNm]	Δq [KN/m]
2	14756.32	12468.27	2288.05	11.33
3	14579.33	13001.89	1577.44	7.84
Case Study	14620.70	13015.36	1605.34	7.97
4	14874.05	12907.14	1966.92	9.88
5	14903.44	13207.17	1696.27	8.58
6	15106.54	13232.55	1873.99	9.55
7	15192.31	13456.44	1735.87	8.9
8	15362.09	13527.65	1834.44	9.49
9	15472.43	13717.12	1755.31	9.14
10	15624.36	13809.71	1814.66	9.52

Two load configurations were defined after the overload was established to be applied to the structure in its various configurations:

- Load Case 0: as the load case in which the eq.(5.4) and eq.(5.5) are applied to the structure to find the values of the maximum and minimum compressive stresses acting on the mid-span cross-section of the edge beam.
- Case Overloaded: as the load case in which in addition to the load combination expressed in eq.(5.4) and eq.(5.5) the value of Δq is applied as a permanent non-structural load (G2) on the edge beam.

The mid-span cross-section of the edge beam is taken as construction detail for the fatigue evaluation. The state of stress in the load case 0 is represented below:

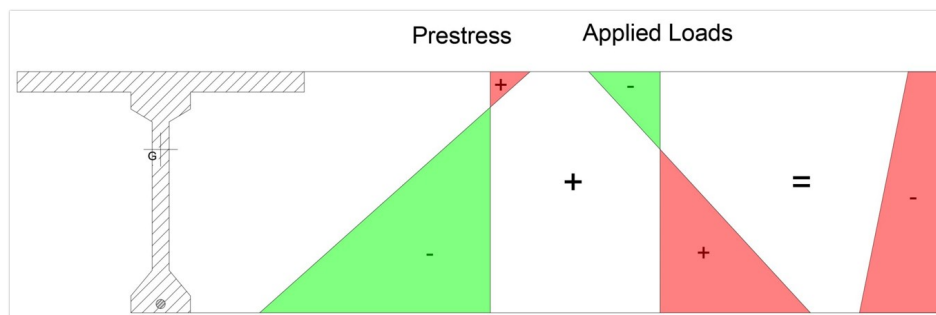


Figure 5.9: State of stress of the mid-span cross-section

The state of stress is the superposition of the effects due to prestress and those due to the application of loads. The result is a constant compression stress acting on the whole section. Considering this representation the application of the overload determines a slope increase in the stress diagram related to the applied load; consequently, the overloaded case shows an increase of the compression at the top of the cross-section, while it presents a reduction in the compression at the bottom. Therefore the stresses are calculated considering the beam extrados.

The obtained values of the maximum and the minimum compressive stress acting on the extrados of the mid-span cross-section of the edge beam are reported:

Maximum and Minimum Compressive stresses				
n°cross-beams	Loas Case 0		Case Overloaded	
	$\sigma_{c,max}$ [MPa]	$\sigma_{c,min}$ [MPa]	$\sigma_{c,max}$ [MPa]	$\sigma_{c,min}$ [MPa]
2	3.83	1.80	4.71	2.68
3	3.73	1.89	4.30	2.46
Case Study	3.73	1.91	4.32	2.50
4	3.90	1.96	4.65	2.71
5	3.91	2.05	4.55	2.69
6	4.03	2.13	4.75	2.85
7	4.08	2.22	4.74	2.85
8	4.18	2.29	4.89	3.00
9	4.24	2.38	4.92	3.06
10	4.33	2.45	5.04	3.17

5.3.3 Definition of concrete S-N curves

Considering the above concerns of the fatigue analysis techniques for concrete that can be applied to existing constructions, the S-N approach is chosen. As already mentioned the fatigue behaviour of concrete is still affected by lack of knowledge, but still, there are some studies which give S-N curve models for different concrete classes. In this study two models are considered: the S-N curves proposed by Jin-Keun Kim and Yun-Young Kim in 1996 [27] and the S-N curves provided by the Fib Model Code 2010 [47].

5.3.3.1 Kim & Kim proposal

Kim and Kim (1996, Korea advanced institute of science and technology) [27] investigated the impact of concrete compressive strength on fatigue life. They suggested an S-N relationship that also considered the compressive strength of concrete. After performing fatigue and strain rate tests they proposed the following S-N relationship:

$$S_{max} = -7.6 \cdot \left(\frac{f_c}{f_l}\right)^{0.066} \cdot \log N_f + 126 \cdot \left(\frac{f_c}{f_l}\right)^{-0.025} \quad (5.6)$$

in which:

- S_{max} is a percentage expressing the degree of utilisation of the compressive strength of the concrete class;
- f_l is a constant equal to 1 MPa;
- f_c is the characteristic compressive strength of the concrete class, in this study will be assumed equal to f_{cd}

Considering the concrete class C35/45 with the related material properties already reported in the chapter 3, the obtained S-N curve is showed below:

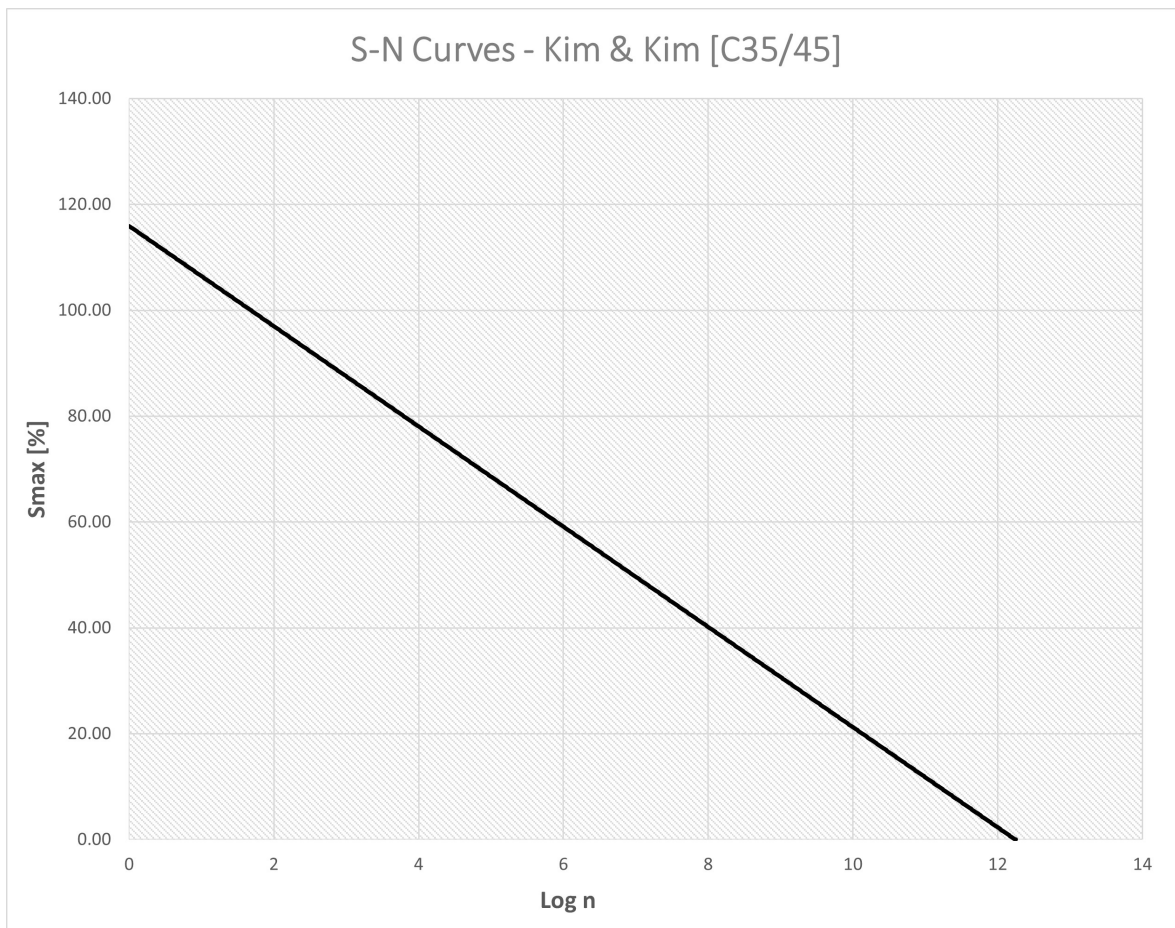


Figure 5.10: S-N curve (Kim&Kim) [27]

The curve represents the relationship between S_{max} and the logarithm of the number of

cycles (n). This model's main drawback is related to the limited number of specimens that were tested to obtain the relationship expressed in eq.(5.6).

5.3.3.2 Fib Model Code 2010

The fib Model Code 2010 [47], covers every aspect of concrete structures entire life cycle, including conceptual design, construction, maintenance, and dismantling, and is the most comprehensive code available. For both national and international code committees, practitioners, and researchers, it is expected to become a significant document[47]. It gives a valid relationship between S_{max} , S_{min} and the logarithm of the number of cycles:

$$\log N_1 = \frac{8}{Y-1} \cdot (S_{c,max} - 1) \quad (5.7)$$

$$\log N_2 = 8 + \frac{8 \cdot \ln(10)}{Y-1} \cdot (Y - S_{c,min}) \cdot \log \left(\frac{S_{c,max} - S_{c,min}}{Y - S_{c,min}} \right) \quad (5.8)$$

with:

$$Y = \frac{0.45 + 1.8 \cdot S_{c,min}}{1 + 1.8 \cdot S_{c,min} - 0.3 \cdot S_{c,min}^2} \quad (5.9)$$

and:

$$S_{c,max} = \frac{|\sigma_{c,max}|}{f_{ck,fat}} \quad (5.10)$$

$$S_{c,min} = \frac{|\sigma_{c,min}|}{f_{ck,fat}} \quad (5.11)$$

If $\log N_1 \leq 8$, then $\log N = \log N_1$, else, if $\log N_1 > 8$, then $\log N = \log N_2$. $f_{ck,fat}$ is the fatigue reference compressive strength calculated as follows:

$$f_{ck,fat} = \beta_{cc}(t) \cdot \beta_{c,sus}(t, t_0) \cdot f_{ck} \cdot \left(1 - \frac{f_{ck}}{250} \right) \quad (5.12)$$

for which:

- f_{ck} is the characteristic concrete compressive strength, which can be assumed as f_{cd} ;
- $\beta_{cc}(t)$ describes the strength development as function of time, where s is a coefficient

that depends upon the concrete class, for C35/45 is equal to 0.20; t is the concrete age expressed in days;

- $\beta_{c,sus}(t, t_0)$ is equal 0.85 for fatigue.

Assuming the equations reported above, the S-N curve for concrete C35/45 is defined:

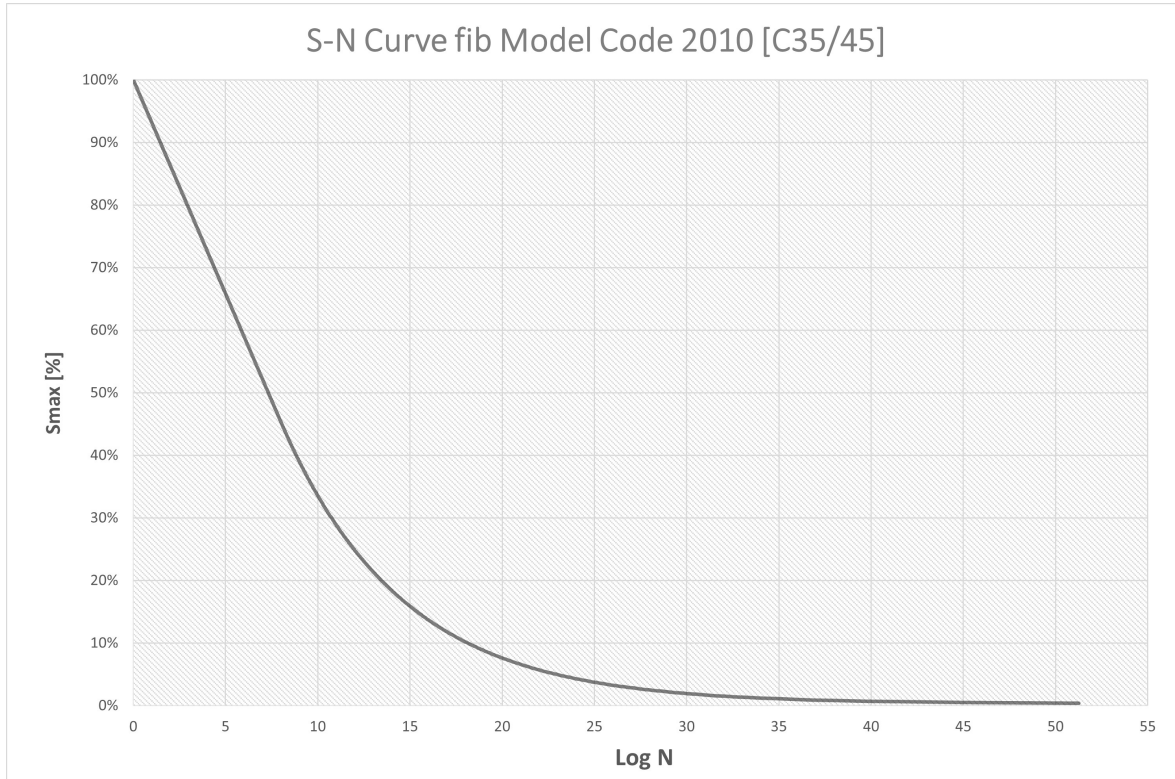


Figure 5.11: S-N curve (fib Model Code 2010)

The S-N relationships were created by testing concrete that had an ultra-high strength (up to C200), and they were then verified for concrete that had a high strength and a regular strength. The curves asymptotically approach the minimum stress level of the corresponding curve when $\log N > 8$ [29].

5.3.4 Discussion of the obtained results

The results for the case study in terms of the number of cycles (N) are reported considering the S-N curves provided by Kim & Kim and by the fib Model Code 2010. Then a comparison between the results obtained for all the different configurations of the cross-beams for both fib Model and Kim&Kim are reported.

5.3.4.1 Kim&Kim S-N curves results

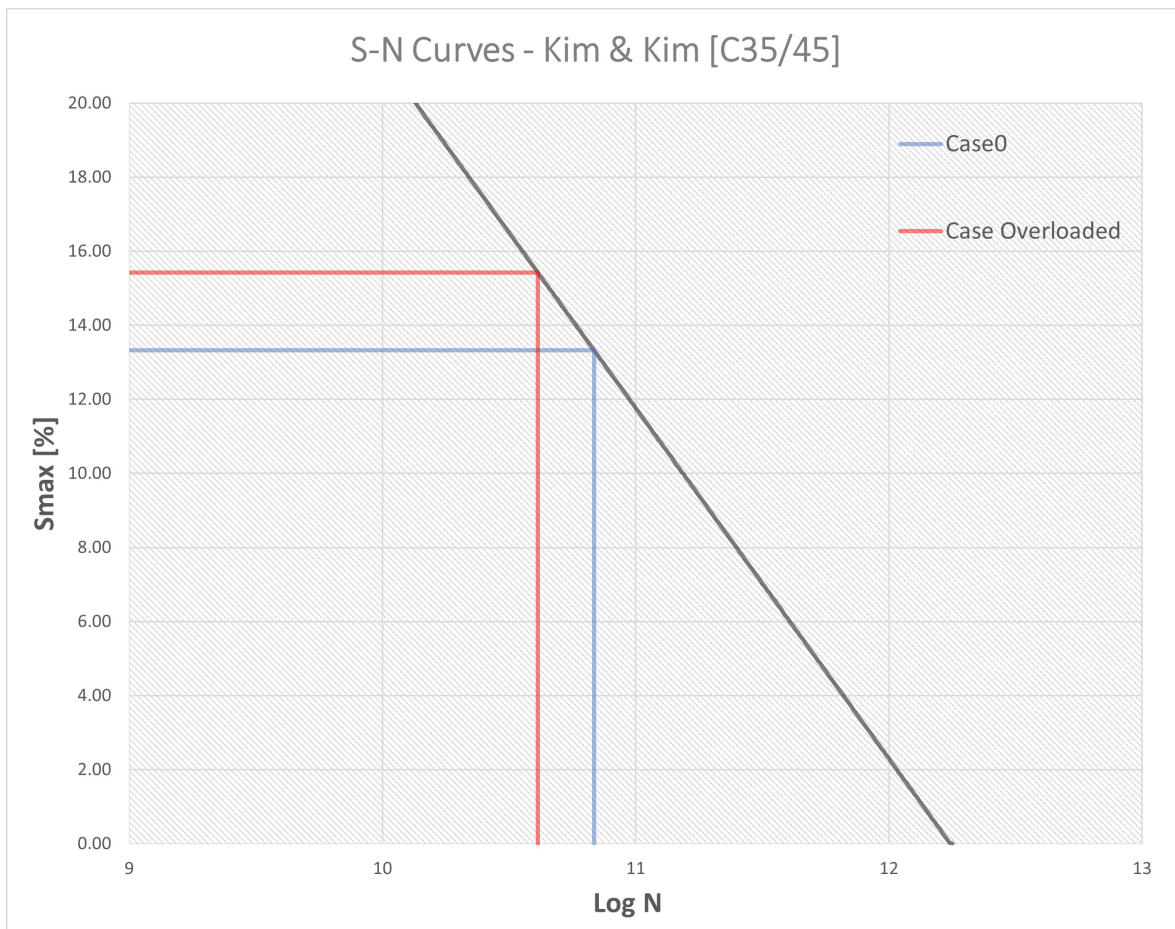


Figure 5.12: Kim&Kim results for study case

It is evident that the concrete's compressive strength is being employed more consistently in the case of overloading, which results in a reduction in the number of fatigue cycles the detail can withstand before failing;

Load Case 0		Case Overloaded		ΔN
LogN	N	LogN	N	
10.84	$6.85 \cdot 10^{10}$	10.61	$4.10 \cdot 10^{10}$	$2.75 \cdot 10^{10}$

despite this, the order of magnitude of the number of cycles value exceeds 10^7 , which is the threshold below which the construction detail can be thought of as having a finite fatigue life.

5.3.4.2 fib Model Code 2010 S-N curves results

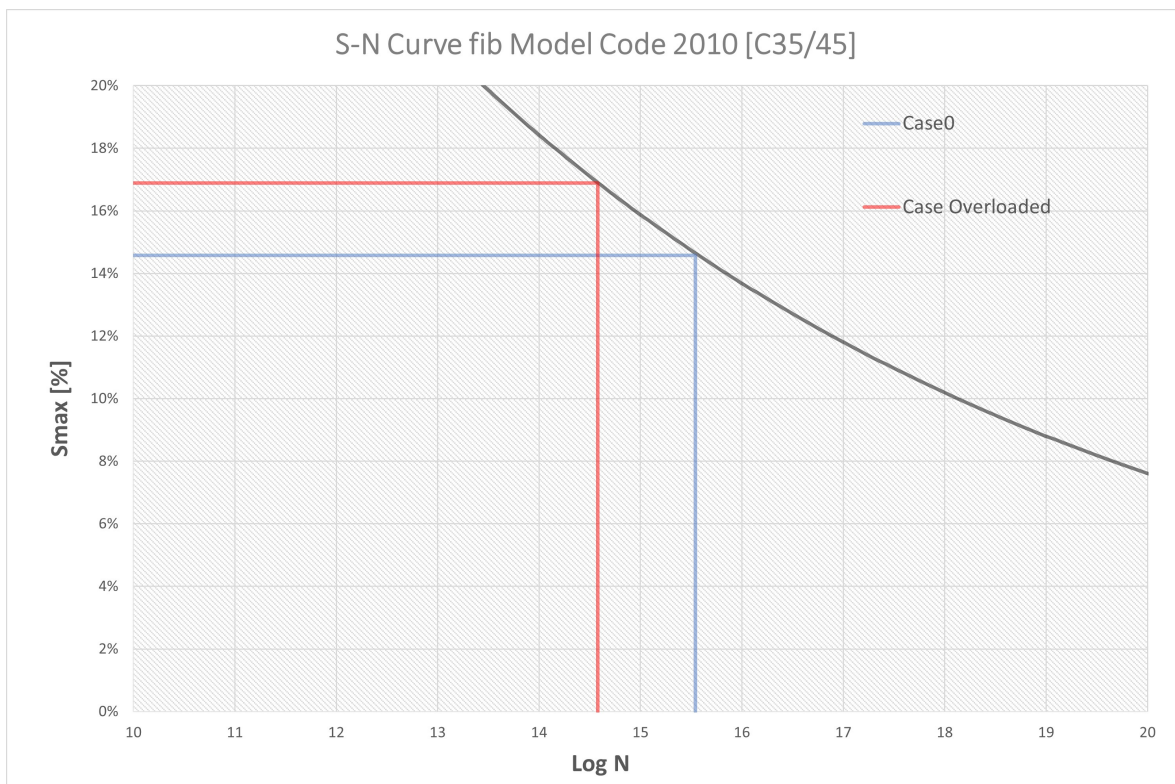


Figure 5.13: fib Model Code results for study case

The S-N curve defined using the fib Model Code 2010 exhibits a higher utilisation of the concrete compressive strength in the overloaded scenario and a corresponding decrease in the number of cycles up to failure as well:

Load Case 0		Case Overloaded		ΔN
LogN	N	LogN	N	
15.54	$3.49 \cdot 10^{15}$	14.58	$3.80 \cdot 10^{14}$	$3.11 \cdot 10^{15}$

Also in this case the order of magnitude of the number of cycles value exceeds 10^7 .

5.3.4.3 Models Comparison

Both the Kim&Kim S-N curve and fib Model code S-N curve show the same behaviour: the application of the overload (Δq), which was used to represent the inefficiency of transverse load distribution entrusted to the cross-beams, determines an increase in the utilization of the concrete compressive strength and consequently, it reduces the number of cycles necessary to reach the fatigue failure of the construction detail. It is noted, however, that the two S-N curve models have different returning values: in particular, the curves presented by Kim&Kim demonstrate a noticeably reduced value of the number of cycles to failure due to fatigue with the same percentage of use of the concrete's compressive strength concerning the ones defined by the fib Model Code. This difference is mainly due to the lower number of tested specimens by Kim&Kim during the definition of the relationship 5.6, on the other hand, the fib model code is the first provision that is truly based on comparison with experimental findings on a significant number of high strength concrete specimens [29]. The same procedure for the case study was performed changing the cross-beam number, the results are reported and commented:

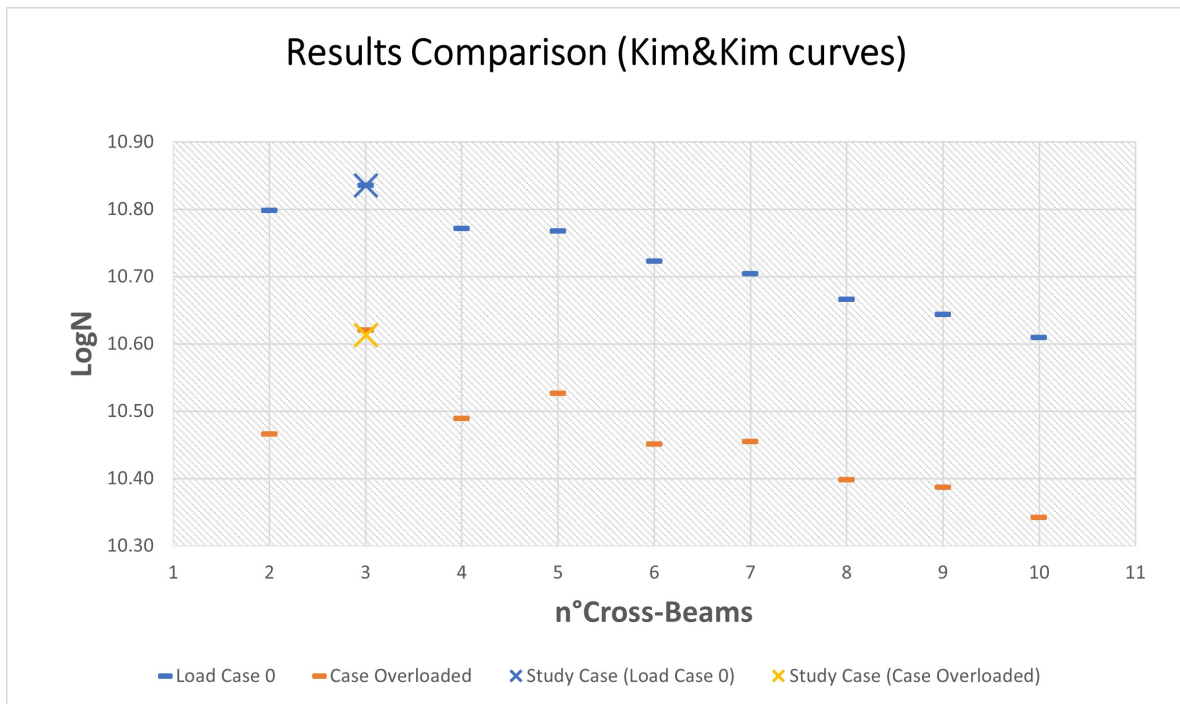


Figure 5.14: Kim&Kim results comparison

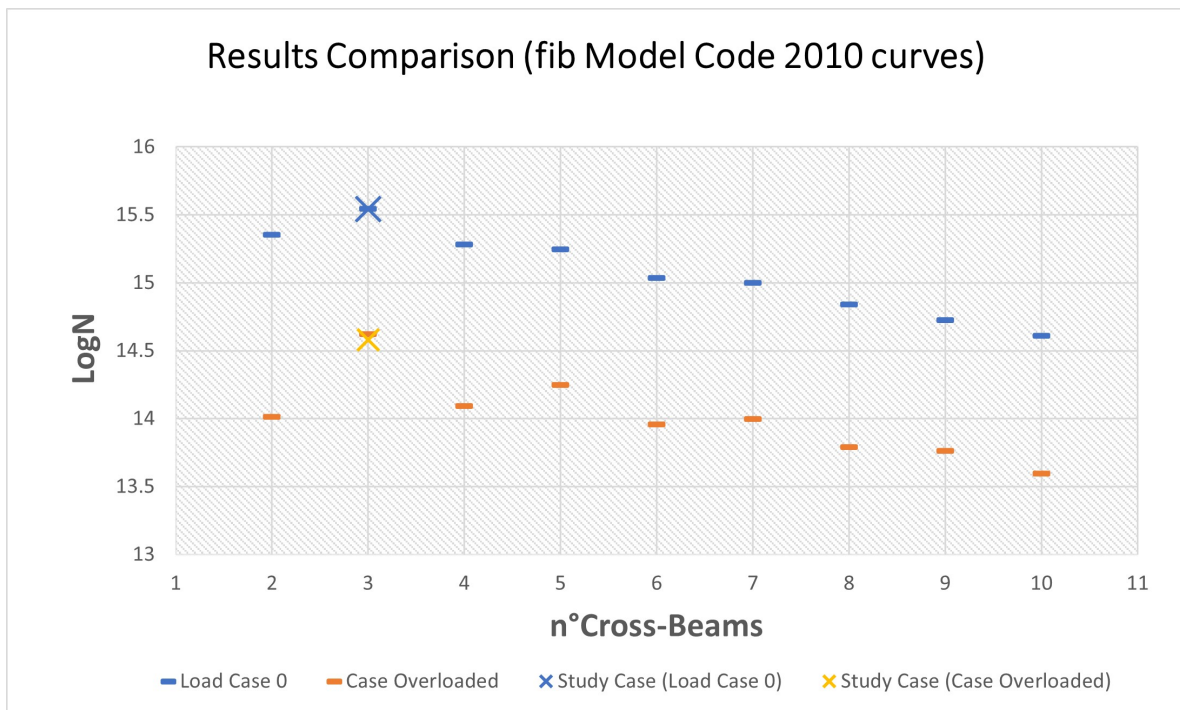


Figure 5.15: fib Model Code results comparison

Disregarding the two models' disparate levels of precision, a certain repeatability of the results can be found in both. The application of the overloaded model, which is representing the amount of bending moment distributed transversely by the cross-beams, determines in all configurations a decrease in the number of cycles necessary to reach fatigue failure for concrete at the extrados of the edge beam. It can then be noted that the cross-beam configuration of the case study gives the best results, as it has a value of the number of cycles in the Load Case 0 greater than all the other configurations. If the initial value of the number of cycles is close to the upper limit of the limited fatigue life, this leads to higher safety. In addition to this, it should be emphasized that as the number of cross-beams increases, the value of $\log N$ in the case 0 tends to decrease, this can be justified by the fact that by increasing the number of cross-beams, the self-weight of the structure inexorably increases. Finally, it can be noted how the configuration with two cross-beams is particularly disadvantaged by the application of the overload, arriving at having a very low value of $\log N$ in the overloaded case and comparable to configurations having a higher number of cross-beams.

Conclusions

In Italy, the majority of the existing bridges and viaducts constructed between the 1960s and 1980s are reaching the end of their service life. In addition, vehicles and transports in general underwent an abrupt increase in size, weight and capacity. This has resulted in a particularly considerable increase in road traffic. The phenomenon of fatigue is a permanent, progressive and localized process of structural change in a material subjected to time-varying stress and strain conditions which can lead to cracking and/or fracture after a sufficient number of cycles. On beam bridges, the fatigue phenomenon is influenced by traffic loads and can lead to the failure of certain construction details without them having reached the end of their service life or having been subjected to loads exceeding their design strengths.

Although the fatigue phenomena have been noted in numerous experiments, there aren't many documented instances of fatigue-related damage to bridge concrete slabs. This may be explained by the inability to discriminate between fatigue cracks in concrete and cracks caused by other types of concrete deterioration, as well as the inability to see fatigue cracks in the steel reinforcement.

The present research is meant to analyse the influence of the transverse beams in the load distribution in an existing beam bridge and to highlight the function that transverse loads distribution plays in beam bridges susceptible to traffic loads that cause the fatigue phenomenon. This was accomplished by examining several case study configurations to determine how the number of transverse beams affected the difference in applied bending moment between the edge beam and the interior beam. Thereafter the structure's fatigue behaviour in its various configurations was investigated. This was achieved by employing the S-N curve approach, which establishes a relationship between the stresses applied on a

structural detail and the number of repetitive cycles necessary for fatigue failure. The values of the number of cycles from 10^4 to 10^7 were assumed as representative of the range within which the construction detail is considered as having a limited fatigue life. The compression acting on the concrete on the extrados of the edge beam was examined and, through the use of an overload that is a representation of the hyperstaticity of the main beams provided by the cross-beams, the influence of the transversal distribution was incorporated.

The outcomes found indicate that the transversal distribution of loads in a beam bridge is influenced by the number and the performance of cross-beams. The stresses acting on the edge beams increase as the transverse beams decrease in number or performance. This rise in stress leads to a reduction in the maximum number of fatigue cycles that the construction detail can withstand, which could result in the development of fatigue cracks. Nevertheless, as the number of cycles obtained in the various configurations evaluated exceeds the value of 10^7 , it can be concluded from the obtained results that the studied structure does not present issues with fatigue.

The main limitation of this study is linked to the fact that the number of cross-beams was considered as the only parameter, leaving out other possible variables related to the geometry of the deck, the stiffness of the structural elements or even the aggressive environmental conditions acting on concrete. However, similar behaviour may be expected for what concern the relationship between the number of cross-beams and the fatigue behaviour of concrete in structures similar to the one analysed.

Bibliography

- [1] ANSI/ASTM. “American Society for Testing Materials - ASTM”. In: E206-72 (1979).
- [2] Tony Bancroft and Barry Cook. *Mulan*. United States: Walt Disney Studios, 1998.
- [3] Riccardo Barsotti and Maurizio Froli. “Statistical analysis of thermal actions on a concrete segmental box-girder bridge”. In: *Structural Engineering International* 10.2 (2000), pp. 111–116.
- [4] Imane Bayane et al. “Quantification of traffic and temperature effects on the fatigue safety of a reinforced-concrete bridge deck based on monitoring data”. In: *Engineering Structures* 196 (2019), p. 109357.
- [5] Sushmita Borah, Amin Al-Habaibeh, and Rolands Kromanis. “The Effect of Temperature Variation on Bridges—A Literature Review”. In: *Energy and Sustainable Futures* (2021), pp. 207–212.
- [6] Britannica. *Encyclopedia Britannica*. The Editors of Encyclopaedia, 2006.
- [7] Byggtjänst. *Betonghandbok Material*. Solna, 1994.
- [8] Daniele Cantelmi. “Effetto dei carichi eccezionali su strutture da ponte= Transit of exceptional vehicles: effects on bridges”. PhD thesis. Politecnico di Torino, 2020.
- [9] Colm Carey and DIT BOLTON STREET. “Traffic Loading on Highway Bridges”. PhD thesis. PhD Thesis, Dublin Institute of Technology, 2008.
- [10] A Carini, O. De Donato, and F. Genna. *Introduzione al metodo degli elementi finiti*. Progetto Leonardo, 1996.

- [11] Circolare del Consiglio Superiore del Ministero dei LL.PP. “Norme relative ai carichi per il calcolo dei ponti stradali”. In: 384 (1962).
- [12] Alberto Corigliano and Alberto Taliercio. *Meccanica computazionale: soluzione del problema elastico lineare*. Società Editrice Esculapio, 2006.
- [13] HAW Cornelissen and HW Reinhardt. “Uniaxial tensile fatigue failure of concrete under constant-amplitude and programme loading”. In: *Magazine of concrete Research* 36.129 (1984), pp. 216–226.
- [14] Ing. Eugenio Coronati. *Ponti a Grigliato diagnosi degradi strutturali criteri e priorità di ispezzionamento*. Clarendon Press, 1981.
- [15] Pietro Croce. “Background to fatigue load models for Eurocode 1: Part 2 Traffic Loads”. In: *Progress in Structural Engineering and Materials* 3.4 (2001), pp. 335–345.
- [16] Krzysztof Dyduch, Maria Szerszeń, and Jean-François Destrebecq. “Experimental investigation of the fatigue strength of plain concrete under high compressive loading”. In: *Materials and Structures* 27 (1994), pp. 505–509.
- [17] Gianni Italsider Falchi Delitala. *La ripartizione trasversale dei carichi negli impalcati da ponte : applicazioni dei metodi di Courbon, Massonet, Bares-Massonet al calcolo delle sollecitazioni nelle travi e traverse*. Italsider, 1972.
- [18] LC la Gasse, RDJM Steenbergen, and DL Allaix. “Traffic load model for road bridges in the urban road network”. In: *Heron* 64.3 (2019), p. 297.
- [19] Frida Göransson and Anna Nordenmark. “Fatigue assessment of concrete foundations for wind power plants”. In: (2011).
- [20] H Gulvanessian. “En1991 eurocode 1: Actions on structures”. In: *Proceedings of the Institution of Civil Engineers-Civil Engineering*. Vol. 144. 6. Thomas Telford Ltd. 2001, pp. 14–22.
- [21] SE Harvey, PG Marsh, and WW Gerberich. “Atomic force microscopy and modeling of fatigue crack initiation in metals”. In: *Acta metallurgica et materialia* 42.10 (1994), pp. 3493–3502.

- [22] Dirk Arend Hordijk. “Local approach to fatigue of concrete.” In: (1993).
- [23] Thomas TC Hsu. “Fatigue of plain concrete”. In: *Journal Proceedings*. Vol. 78. 4. 1981, pp. 292–305.
- [24] Ulrika Johansson. “Fatigue tests and analysis of reinforced concrete bridge deck models”. PhD thesis. Bygghvetenskap, 2004.
- [25] Fatima Zahraa Kachkouch et al. “Fatigue behavior of concrete: A literature review on the main relevant parameters”. In: *Construction and Building Materials* (2022).
- [26] JJ Kauzlarich. “The Palmgren-Miner rule derived”. In: *Tribology Series*. Vol. 14. Elsevier, 1989, pp. 175–179.
- [27] Jin-Keun Kim and Yun-Yong Kim. “Experimental study of the fatigue behavior of high strength concrete”. In: *Cement and Concrete Research* 26.10 (1996), pp. 1513–1523.
- [28] Susumu Kono et al. “Low cycle fatigue characteristics of high strength concrete”. In: *Proceedings of the 8th International Symposium on Utilization of High-Strength and High-Performance Concrete, Tokyo, Japan*. 2008, pp. 27–29.
- [29] EOL Lantsoght. “Fatigue of concrete under compression: Database and proposal for high strength concrete”. In: *Report nr. 25.5-14-04* (2014).
- [30] Algernon Charles Liebenberg. *Concrete bridges: design and construction*. Longman Scientific and Technical, 1992.
- [31] Niels Christian Lind, Mayasandra Krishnappa Ravindra, and John Power. “A review of the effective width formula”. In: (1971).
- [32] Alessandro Lipari, Eugene J. O’Brien, and Colin C. Capriani. “A comparative study of a bridge traffic load effect using micro-simulation and Eurocode load models”. In: 2012.
- [33] Mattia Mairone. “STUDIO DI UN VIADOTTO ESISTENTE CON IMPALCATO A CASSONE IN ACCIAIO A PIASTRA ORTOTROPA= STUDY OF AN EXISTING VIADUCT WITH BOX-GIRDER ORTHOTROPIC STEEL DECK”. PhD thesis. Politecnico di Torino, 2021.

- [34] Johan Maljaars. “Evaluation of traffic load models for fatigue verification of European road bridges”. In: *Engineering Structures* 225 (2020), p. 111326.
- [35] MA Masrom and LD Goh. “Comparative study of bridge traffic loadings between British standards and Eurocodes”. In: *AIP Conference Proceedings*. Vol. 2020. 1. AIP Publishing LLC. 2018, p. 020037.
- [36] Polana Nagendra et al. “T-BEAM DECK SLAB BRIDGE ANALYSIS”. In: 2018.
- [37] U. Nürnberger. “Schwingfestigkeitsverhalten von Betonstählen”. In: *IABSE Report 37* (1982), pp. 213–220.
- [38] Alain Nussbaumer, Luis Borges, and Laurence Davaine. *Fatigue design of steel and composite structures: Eurocode 3: Design of steel structures, part 1-9 fatigue; Eurocode 4: Design of composite steel and concrete structures*. John Wiley & Sons, 2012.
- [39] Francesca Maria Pavone. “Structural behavior of prestressed bridges under corrosion damage”. PhD thesis. Politecnico di Torino, 2018.
- [40] Michel Prat. “Traffic load models for bridge design: recent developments and research”. In: *Progress in Structural Engineering and Materials* 3.4 (2001), pp. 326–334.
- [41] Sabeeh Z Al-Sarraf, Ammar A Ali, and Rana A Al-Dujaili. “Analysis of composite bridge superstructures using modified grillage method”. In: *Eng. Tech. J* 27.5 (2009), pp. 942–952.
- [42] Max Schläfli and Eugen Brühwiler. “Fatigue of existing reinforced concrete bridge deck slabs”. In: *Engineering structures* 20.11 (1998), pp. 991–998.
- [43] R Shreedhar and Spurti Mamadapur. “Analysis of T-beam bridge using finite element method”. In: *International Journal of Engineering and Innovative Technology (IJEIT)* 2.3 (2012), pp. 340–346.
- [44] Peter Sivák and Eva Ostertagová. “Evaluation of fatigue tests by means of mathematical statistics”. In: *Procedia Engineering* 48 (2012), pp. 636–642.
- [45] Dominik Skokandić et al. “Modelling of traffic load effects in the assessment of existing road bridges”. In: *Grđevinar* 71.12. (2019), pp. 1153–1165.

- [46] British Standard. “Eurocode 2: Design of concrete structures—”. In: *Part 1.1* (2004), p. 230.
- [47] Luc Taerwe, Stijn Matthys, et al. *Fib model code for concrete structures 2010*. 2013.
- [48] Thomas E Tischer and John A Kuprenas. “Bridge falsework productivity—Measurement and influences”. In: *Journal of construction engineering and management* 129.3 (2003), pp. 243–250.
- [49] Ministero delle Infrastrutture e dei Trasporti. “NTC 2018-Norme Tecniche per le Costruzioni di cui al DM 17/01/2018”. In: *Gazzetta Ufficiale* 42 (2018).
- [50] WF Wu, HY Liou, and HC Tse. “Estimation of fatigue damage and fatigue life of components under random loading”. In: *International journal of pressure vessels and piping* 72.3 (1997), pp. 243–249.
- [51] Mohamed A Youssef, Chimay J Anumba, and Tony Thorpe. “Intelligent selection of concrete bridge construction methods in Egypt”. In: (2005), pp. 1–14.
- [52] GY Zhao, PG Wu, and LM Bai. “Research on fatigue behaviour of high-strength concrete under compressive cyclic loading”. In: *Proceeding of the 4th International Symposium on Utilization of High-strength/High-performance concrete, Paris, France*. 1996, pp. 29–31.

Acronyms

FEA Finite Element Analysis

DOF Degree of Freedom

ULS Ultimate Limit State

FEM Finite Element Method

FE Finite Element

LM1 Load Model 1

LM2 Load Model 2

LM3 Load Model 3

FLM1 Fatigue Load Model 1

FLM2 Fatigue Load Model 2

FLM3 Fatigue Load Model 3

FLM4 Fatigue Load Model 4

ASTM American Society for Testing
Materials